Autonomic Neuroscience: Basic and Clinical 220 (2019) 102558

Contents lists available at ScienceDirect

Autonomic Neuroscience: Basic and Clinical

journal homepage: www.elsevier.com/locate/autneu

# Changes in excitability and ion channel expression in neurons of the major pelvic ganglion in female type II diabetic mice

Michael Gray[a,1], Kawasi M. Lett[a,1], Virginia B. Garcia[a], Cindy W. Kyi[a], Kathleen A. Pennington[b], Laura C. Schulz[b], David J. Schulz[a,*]

[a] Division of Biological Sciences, University of Missouri, Columbia, MO 65211, USA
[b] Department of Obstetrics, Gynecology and Women's Health, University of Missouri, Columbia, MO 65211, USA

ABSTRACT

Bladder cystopathy and autonomic dysfunction are common complications of diabetes, and have been associated with changes in ganglionic transmission and some measures of neuronal excitability in male mice. To determine whether type II diabetes also impacts excitability of ganglionic neurons in females, we investigated neuronal excitability and firing properties, as well as underlying ion channel expression, in major pelvic ganglion (MPG) neurons in control, 10-week, and 21-week *Lepr*$^{db/db}$ mice. Type II diabetes in *Lepr*$^{db/db}$ animals caused a non-linear change in excitability and firing properties of MPG neurons. At 10 weeks, cells exhibited increased excitability as demonstrated by an increased likelihood of firing multiple spikes upon depolarization, decreased rebound spike latency, and overall narrower action potential half-widths as a result of increased depolarization and repolarization slopes. Conversely, at 21 weeks MPG neurons of *Lepr*$^{db/db}$ mice reversed these changes, with spiking patterns and action-potential properties largely returning to control levels. These changes are associated with numerous time-specific changes in calcium, sodium, and potassium channel subunit mRNA levels. However, Principal Components Analysis of channel expression patterns revealed that rectification of excitability is not simply a return to control levels, but rather a distinct ion channel expression profile in 21-week *Lepr*$^{db/db}$ neurons. These data indicate that type II diabetes can impact the excitability of post-ganglionic, autonomic neurons of female mice, and suggest that the non-linear progression of these properties with diabetes may be the result of compensatory changes in channel expression that act to rectify disrupted firing patterns of *Lepr*$^{db/db}$ MPG neurons.

## 1. Introduction

Diabetes is a systemic, progressive disease characterized by lack of insulin directly (Type I), or functional lack of its effectors and/or insulin resistance (Type II), that ultimately leads to hyperglycemia and chronic complications. Diabetes is the seventh leading cause of death in the United States and afflicts 11.1–11.9% of adults over the age of 20; this rate has increased from 8.9% in years 1988–1994 to 11.9% in years 2011–2014 (United States. Department of Health and Human Services et al., 2016). In addition, diabetic complications are age dependent (Gunnarsson, 1975; DCCT Research Group, 1996; Liu et al., 2017). This age dependence combined with the 111.5% increase in persons age 65 and older from 1975 to 2015 (United States. Department of Health and Human Services. et al. 2016), necessitates studying an important complication of diabetes—diabetic neuropathy.

Diabetic neuropathy is particularly dangerous due to its insidious development, susceptibility of autonomic neurons and their subsequent regulation of vital organ systems, and a potential for positive feedback loops through dysregulation of microvasculature (Faerman et al., 1971; Vinik et al., 2003). Interventions are difficult as symptoms are subclinical and are often undiagnosed until long after neural lesions occur. That is, autonomic motor neuron damage occurs long before patients report sensory symptoms. This is supported by the finding that in diabetic mice, thin, non-myelinated post ganglionic autonomic motor neurons show deficits long before either sensory or motor neurons do (Liu et al., 2017). Neuropathic lesions can affect various autonomic pathways resulting in gastroparesis (Vinik et al., 2003), cardiovascular dysregulation (Vinik et al., 2003, 2011), sudomotor dysfunction (Liu et al., 2017), diabetic cystopathy (Faerman et al., 1971; Frimodt-Moller, 1980; Kaplan et al., 1995; Vinik et al., 2003), and dysregulation of blood flow in the periphery (UKPDS, 1998). Bladder dysfunction as a result of diabetes (i.e. diabetic cystopathy) is characterized by reduced bladder sensation, increased post-residual void volume and overactive bladder (Kaplan et al., 1995; Yuan et al., 2015), and was first formally described in diabetics in 1864 (Faerman et al., 1971). Some of the effects of diabetic cystopathy can be attributed to damaged bladder afferents. For example, it has been shown in streptozocin (STZ) treated rats (type I diabetes model) that diabetic cystopathy is correlated with reduced levels of nerve growth factor (NGF) in dorsal root ganglion neurons (Sasaki et al., 2002). Furthermore, when NGF is expressed at

* Corresponding author at: Division of Biological Sciences, University of Missouri-Columbia, 218 LeFevre Hall, Columbia, MO 65211, USA.
*E-mail address:* schulzd@missouri.edu (D.J. Schulz).
[1] Denotes equal contribution by these authors.

https://doi.org/10.1016/j.autneu.2019.102558
Received 11 October 2018; Received in revised form 5 June 2019; Accepted 12 June 2019

the bladder wall, the development of diabetic cystopathy and subsequent increased post residual void volume can be mitigated (Sasaki et al., 2004). However, little is known as to how diabetes impacts autonomic neurons innervating the bladder, lower bowel, and urogenital organs, and how this contributes to lower gastrointestinal problems, bladder cystopathy and reproductive dysfunction.

The major pelvic ganglion (MPG) of the mouse is the primary motor innervation of the urinary bladder, lower bowel and reproductive organs. When examining motor neurons of this network in males, Tompkins et al. (2013), found that in post-ganglionic, MPG neurons in BKS Lepr$^{db/db}$ mice, a model for type II diabetes, had an enhanced number of excitatory post-synaptic potentials (EPSP) up to 20 s after pelvic nerve stimulation relative to control. Simultaneously, the authors observed no change in EPSP amplitude. However, STZ-treated mice, a model for type I diabetes, did not differ in EPSP number and had significantly reduced amplitudes relative to control mice. This suggests that the type I and type II models are distinct in how they affect physiology of MPG neurons. Furthermore, change in action potential properties is similarly dependent on diabetic type: after-hyperpolarization (AHP) duration was significantly decreased in Lepr$^{db/db}$ mice, while being significantly increased in STZ mice (Tompkins et al., 2013). Finally, MPG neuron input resistance ($R_{IN}$) and resting membrane potential (RMP) are decreased and depolarized, respectively, in Lepr$^{db/db}$ mice but unaffected in STZ mice (Tompkins et al., 2013). These results suggest that both EPSP and intrinsic properties of MPG neurons are differentially modulated by the nature of the diabetic model. All of these data were collected in male mice, and thus far no study has examined the impact of any diabetic model on neurons of the female MPG.

In this study, we exploit the Lepr$^{db/db}$ C57BL/6J mouse, to extend our understanding of how type II diabetes affects in neuronal excitability in neurons of the MPG of female mice. Specifically, we examine firing properties of neurons at 10- and 21-week time points in diabetic animals by combining current clamp recordings of neuronal output with ion channel expression analyses in the MPGs of female mice. We predicted that intrinsic properties should resemble that observed by Tompkins et al. (2013); an increased RMP, decreased $R_{IN}$, and decreased AHP duration. Despite there being no change in EPSP amplitude, Tompkins et al. (2013), also observed increased number of EPSPs up to 20s after stimulation, and ectopic spikes after stimulation. Therefore, we expected that excitability would be increased in diabetic conditions. However, we observed a distinct effect: excitability of MPG neurons was initially increased at 10-weeks, but subsequently became less excitable again – towards baseline levels – at 21-weeks. These results suggest a compensatory change in MPG neurons in diabetic animals. We then went on to investigate potential underlying mechanisms for these changes via measurements of ion channel mRNA levels in MPGs from 10-week and 21-week diabetic females.

## 2. Materials and methods

### 2.1. Type II Diabetes Model – Lepr$^{db/db}$ animals

Wild type (WT) C57BL/6J and Lepr$^{db/db}$ (B6.BKS(D)-Lepr$^{db}$/J) female mice (*Mus musculus*) were obtained from the Jackson Laboratory (Bar Harbor, ME, USA). Lepr$^{db/db}$ mice have a mutation that interrupts the longest isoform of the leptin receptor (Chen et al., 1996). These animals display hyperphagia, obesity, hyperglycemia and hyperinsulinemia, which has led to their widespread use as a model of type II diabetes. Together, mouse and rat leptin mutants have been used in over 4000 published studies of type II diabetes (Wang et al., 2014). Lepr$^{db/db}$ mice have been used by the Animal Models of Diabetic Complications Consortium and others as models for diabetic neuropathy (Sullivan et al., 2007).

Mice were group housed in cages on a 12 h light/dark cycle and fed a standard chow diet ad libitum. All animal procedures were performed in accordance with National Institutes of Health Guide for the Care and Use of Laboratory Animals and approved by the University of Missouri Animal Care and Use Committee.

### 2.2. Establishing a diabetic phenotype

#### 2.2.1. Glucose measurement

Mice used in this study were aged 9–10 weeks (10-week group) or 20–21 weeks (21-week group). Individuals from the 10-week (n = 15 WT and n = 14 Lepr$^{db/db}$) and 21-week (n = 6 WT and n = 14 Lepr$^{db/db}$) groups were fasted for 4 h and then a fasting glucose measurement was taken via tail blood using the average of two readings of a OneTouch® (Sunnyvale, CA) or ReliOn Prime® (Arkay inc., Kyoto, Japan; Distributed by Walmart, Bentonville, AR) Blood Glucose Monitoring System. At this time blood was collected to measure fasting serum insulin levels. Weights were also recorded at this time.

#### 2.2.2. Insulin Elisa

Serum insulin levels were analyzed using a Mouse/Rat Insulin Elisa (Millipore™, Billerica, MA) according to manufacturer's instructions. A total number of 7 samples at 10 weeks were run for both WT and Lepr$^{db/db}$ females. At 21 weeks of age 10 Lepr$^{db/db}$ and 6 WT females were analyzed. For Lepr$^{db/db}$ serum was diluted at 1:20 with matrix solution provided in the ELSIA kit to allow for measurements to fall on the standard curve.

### 2.3. Electrophysiology

MPGs were dissected from isoflurane euthanized female mice from wildtypes (n = 9) at 10 weeks (WT), Lepr$^{db/db}$ at 10 weeks (n = 5; DB10), or Lepr$^{db/db}$ at 21 weeks (n = 5; DB21). Dissection and all experiments were done in oxygenated physiological saline at room temperature. MPGs were dissected out and pinned to a Sylgard (Dow, Midland, MI) lined perfusion chamber. The preparation was then desheathed using small pins to remove excess tissue. Neurons of the MPG were impaled randomly. Saline was composed of (in mM): NaCl, 146; KCl, 4.7; $MgSO_4$, 0.6; $NaHCO_3$, 1.6; $NaH_2PO_4$, 0.13; $CaCl_2$, 2.5; Glucose, 7.8; HEPES, 20; pH'd to 7.3. Electrodes were pulled on a P-97 microelectrode puller (Sutter, Novato, CA) filled with 3 M KCl, and had resistances of 30 to 60 MΩ. Recordings were acquired in Bridge mode using an Axoclamp 900A and digitized using a Digidata 1440A using the pClamp 10.3 suite of software (Molecular Devices, Sunnyvale, Ca) running on an IBM-compatible computer. Silver electrode and ground wire were chlorided using household bleach (Clorox, Oakland, CA).

#### 2.3.1. Passive properties

Resistance, time constant, capacitance and rebound spikes were estimated from −500 pA current injections of 400 ms. In some protocols where there were no rebound spikes, these properties were estimated from −500 pA current injections for 2000 ms. To ensure these protocols did not differ, we examined action potential properties for 12 WT neurons where both protocols were used. A paired *t*-test showed that hyperpolarization duration did not significantly affect these measurements, the closest measurement to being affected was AHP ($t(11) = 2.090$, $p = 0.061$) while all other properties were unaffected ($p > 0.1$). In some cells, we observed subthreshold oscillations. To minimize the impact of these oscillations on measurements of passive properties, we used relatively large current injections (−500 pA) rather than −10 to −100 pA typically used (Jobling and Lim, 2008). This measurement led to a slightly smaller estimate (94%) of $R_{IN}$ than when we measured with −50 pA injections, but minimized the influence of oscillations in our measurements. Due to the contamination of slow activating currents and membranes being non-isopotential in real neurons, time constant was estimated by the 2 exponential fit; $V_m(t) = V_{final} + A_1 e^{-t/\tau_1} + A_2 e^{-t/\tau_2}$; the larger A (IR) and time constant term was taken to be the time constant (Golowasch et al., 2009; White

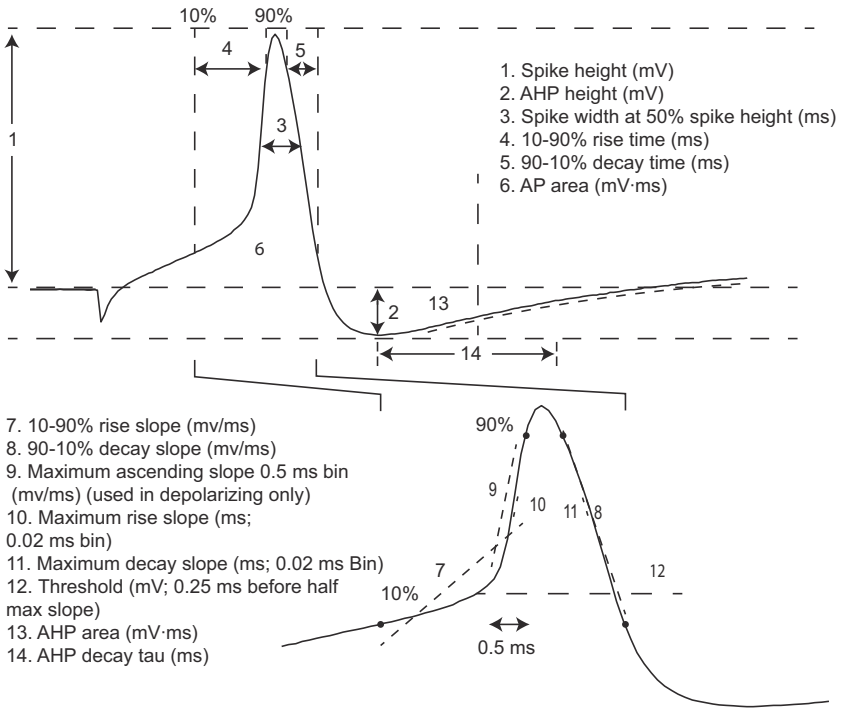


**Fig. 1.** Action potential properties measured from depolarization and rebound induced spikes. Each number corresponds to a given measurement, as described in the Materials and methods. These numbers are referred to in the Results section when relevant.

and Hooper, 2013). Capacitance was estimated from this time constant and $R_{IN}$. For excitability data, current was injected from 0 to 700 pA in 50 pA steps for 400 ms.

### 2.3.2. Action potential properties

Action potential properties were estimated both manually (Spike count, Rheobase, AP slope to depolarizing current injection, and Threshold) and by using the auto-statistics package of the Clampfit program from the pClamp 10.3 suite of software (Molecular Devices, Sunnyvale, Ca) (All others). These properties are illustrated in Fig. 1 for reference, and unless otherwise stated were performed on rebound spikes to prevent contamination from current injection.

### 2.3.3. Threshold measurement

Threshold was measured from two methods and verified by estimation from passive properties and rheobase. First, we extrapolated manually from depolarizing current step protocols. Second, we adopted an adapted version of the spike slope method, where the derivative of voltage with respect to time slope is plotted vs voltage and the voltage at which this slope meets or exceeds some slope is threshold and usually set from 2 to 20 mV/ms (Naundorf et al., 2006; Platkiewicz and Brette, 2010, 2011). However, rather than using constant ascending spike slope, this method was adapted by measuring maximal ascending slope within a 0.5 ms bin, defining threshold as the voltage recorded 0.25 ms before the center point of the half maximal bin. Within wildtype, no significant differences were found between this method (M = −23.5, SD = 8.1, mV) and manual estimation (M = −23.5, SD = 8.1, mV). Slope method was chosen to minimize any confounds between changes in ascending slope.

### 2.3.4. Inclusion and exclusion criterion

The goal of this study was to compare the impact of diabetic condition on excitability, passive, and action potential properties of two groups of diabetic animals with a common control. While sharp electrode recordings are the standard for this preparation (Felix et al., 1998; Lee et al., 2002; Tan et al., 2007; Jobling and Lim, 2008; Tompkins et al., 2010, 2013), all sharp electrode recordings produce impalement damage that is thought to correlate with depolarization of the neuron and introduction of leak (Dale, 1995; Li et al., 2004; Cymbalyuk and Shilnikov, 2005; Springer et al., 2015). In practice, many authors set minimum criteria for RMP, $R_{IN,}$ or both to account for this damage (Tompkins et al., 2010, 2013; Springer et al., 2015). However, we felt that this was inappropriate for this study, as diabetic condition was found to modulate some of these target properties in this study (Fig. 3B) and RMP and $R_{IN}$ in previous studies (Tompkins et al., 2013). Further, as explained in our results, the diabetic condition itself appears to decouple the correlation of these proposed indicators of cell health in the DB21 condition (Fig. 3E). Therefore, our criteria were based on the most depolarized RMP, and minimum $R_{IN}$ of a neuron in the control that produced both rebound and depolarized spikes to hyperpolarizing and depolarizing current injections, respectively.

Some neurons impaled produced no spikes. As we could not ascertain whether this was due to impalement damage, or these cells being silent neurons or closely apposed satellite glial cells (Hanani, 2010), the following inclusion/exclusion criteria were made: 1) All included neurons must produce spikes to depolarizing current injections. 2) All cells must have resting membrane potentials less than −25 mV. 3) All cells must have $R_{IN}$ > 20 MΩ. Inclusion criteria were left fairly broad so as not to bias the population of neurons in each group without an a priori understanding of how diabetes will affect these cells in female mice.

### 2.3.5. Statistics

Data were organized and stored in Microsoft Excel (Microsoft, Redmond, WA). All Statistics and graphs were made in Sigmaplot 11.0 (Chicago, Il), R (https://www.r-project.org/) and formatted in Adobe Illustrator CC 2017 (San Jose, CA). Data that passed normality testing and were shown to be homoscedastic were analyzed using one-way ANOVA. They were plotted as means ± SEM. Most data, however, were found to be non-normal and/or fail equal variance and comparisons were therefore made with a non-parametric Kruskal-Wallis one-way ANOVA on ranks using a post-hoc Dunn's test and plotted as medians

and quartiles with outliers drawn.

### 2.4. qRT-PCR Methods

After each set of experimental recordings of 6–12 h, paired MPGs from each animal were collected into Trizol reagent (Life Technologies, Carlsbad, CA), homogenized, and stored at −80 °C until RNA extraction. Total RNA was isolated from MPGs according to the protocol provided by the manufacturer. Complementary DNA (cDNA) was generated from 100 ng total RNA primed by a mixture of random hexamers and oligo-dT primers. Reverse transcription reactions were carried out at a volume of 20 µl using qScript cDNA SuperMix (QuantaBio, Beverly, MA) according to manufacturer protocols. Following cDNA synthesis, the reaction was heat inactivated and diluted 5× to a final volume of 100 µl before being used as a template for quantitative PCR (qPCR). From each cDNA reaction we quantified at least 15 different gene products. Multiple cDNA synthesis reactions were carried out from a single total RNA sample to quantify the full suite of genes examined in this study.

In our previous work, we designed or modified and independently validated qPCR primers for use in absolute quantitation of mRNA copy number for all of the genes of interest in this study. Most of these primer sets are previously published, and standard curves generated and used as described in our previous work (Garcia et al., 2014, 2018). Table 1 reports each of the ion channel genes assayed for realtime PCR, including the currents to which they contribute, as well as the primer sequences used in the PCR reactions. Briefly, qPCR was carried out using SYBR mastermix (BioRad) according to the manufacturer's instructions, and consisted of primers at final concentrations of 2.5 µM. Reactions were carried out on a CFXConnect (BioRad) machine with a three-step cycle of 95 °C-15 s, 58 °C-20s, 72 °C-20s, followed by a melt curve from 65 °C to 95 °C. Fluorescence data acquisition was made at the 72 °C step, and every 0.5 °C of the melt curve. All reactions were run in triplicate, and the average Ct (cycle threshold) was used for interpolation with standard curves to generate copy number for a given reaction.

The unit we use to express all of the qPCR data in this study is "copy number per ng of total RNA," and reflects the amount of input RNA that went into the cDNA synthesis reaction. All of the data were normalized (see Garcia et al., 2014) relative to the average expression of Glyceraldehyde 3-phosphate dehydrogenase (GAPDH), beta-actin, and hypoxanthine guanine phosphoribosyl transferase (HPRT) genes from each sample (Vandesompele et al., 2002). Samples that were found to have low expression of these control genes were eliminated from the analysis. None of the control genes showed significant differences in expression across groups.

## 3. Results

### 3.1. $Lepr^{db/db}$ mice produce a diabetic phenotype with hyperglycemia that differs according to age

Diabetic neuropathy and the metabolic derangements of diabetes itself (Gunnarsson, 1975; Giachetti, 1978; Medici et al., 1999) are age-dependent. Therefore, we wanted to verify that our $Lepr^{db/db}$ model exhibited diabetic physiological properties such as weight gain, elevated blood sugar and serum insulin to verify our diabetic model had sufficient time to develop the phenotype.

### 3.2. $Lepr^{db/db}$ mice are heavier than WT

Diabetic mice from both 10 to 21 week age groups, were

**Table 1**
Gene identification and primer sets used for realtime PCR reactions to quantify ion channel mRNA levels. Accession numbers provided for each gene of interest. Primer sets were obtained from PrimerBank (Spandidos et al., 2010) or generated de novo using PRIMER3 software. All primer sets were validated before use (see Garcia et al. (2014)).

| Gene name | Accession # | Channel (Current) Type | Forward primer (5′ to 3′) | Reverse Primer (5′ to 3′) |
|---|---|---|---|---|
| *CACNA1A* | NM_007578 | $Ca_v2.1$ (P/Q-type $Ca^{2+}$) | AAAGGCTCCTACCTGAGGAAT | CTCAGTGTCCGTAGGTCAAAC |
| *CACNA1B* | NM_007579 | $Ca_v2.2$ (N-type $Ca^{2+}$) | ACAACGTCGTCCGCAAATAC | CAGGGCCAGAACAATGCAGT |
| *CACNA1C* | NM_001159534 | $Ca_v1.2$ (L-type $Ca^{2+}$) | GGAGGGCGTGCATAAGCATT | AGGAAGAGATACTCCACTCGTTC |
| *CACNA1D* | NM_001083616 | $Ca_v1.3$ (L-type $Ca^{2+}$) | GCTTACGTTAGGAATGGATGGAA | GAAGTGGTCTTAACACTCGGAAG |
| *CACNA1E* | NM_009782 | $Ca_v2.3$ (R-type $Ca^{2+}$) | CAGTCCGGCAGAACTGTTTCA | GAGACATTGGGGTCTTGTCATC |
| *CACNA1G* | NM_001112813 | $Ca_v3.1$ (T-type $Ca^{2+}$) | AGAGTCCGCTGACCATGAAAT | CCGGAATGTGTCGCAGATCA |
| *CACNA1H* | NM_021415 | $Ca_v3.2$ (T-type $Ca^{2+}$) | CTTCAGTAGCATCTCCAAGGC | CAGCCATCCTCGTCAATACTC |
| *KCNA1* | NM_010595 | $K_V1.1$ | CCCCTCCTACCCCTCTTC | CTGCCGCATTCAGACTCT |
| *KCNA2* | NM_008417 | $K_V1.2$ | GTCTGAGCTTCTGCAGGAAA | CCTATTTGTGTATCTGTGCCATC |
| *KCNA3* | NM_008418 | $K_V1.3$ | CTGCCCATTACCTTGTCGTT | CAGTAAAGCCACCTTCTCCA |
| *KCNA4* | NM_021275 | $K_V1.4$ | GAAAGCAGGAAATGAAGAGCATC | GTTGCAGCGTGGAAAAGG |
| *KCNA5* | NM_145983 | $K_V1.5$ | GCAGAGTCTCCAAGCAGAAG | TCTTCGAATACCCAGAAAGCTC |
| *KCNA6* | NM_013568 | $K_V1.6$ | CAGAGAAGTTCAAGATCGGGTA | ATTTCTGCTTGGGATGAGGAC |
| *KCNB1* | NM_008420 | $K_V2.1$ | GGTGGAGAGGACAATGAACA | GAGTTCGACAACACGTGCT |
| *KCNB2* | NM_001098528 | $K_V2.2$ | AAGTGTGTTGAGAGACAGAGC | TTGCTGGAGAAACCTAACTCG |
| *KCNC1* | NM_001112739 | $K_V3.1$ | TTCGGTCTTGTTCACGATGG | CCCTACTCATCCCGCTACG |
| *KCNC2* | NM_001025581 | $K_V3.2$ | TTGTGTCTCCTTTAGTCTGTGC | AACGTGTTTCCTGTTGACGA |
| *KCNC3* | NM_008422 | $K_V3.3$ | CACAATGCTGCTCAGGCT | GAAGACAAGAGCCCAATCACT |
| *KCNC4* | NM_145922 | $K_V3.4$ | CTTGGCAGGTCTCTGTGTT | GGACTATGCCTGTGCTGATG |
| *KCND1* | NM_008423 | Kv4.1 | ATCCGCCTTGCCAACTCTAC | GCTTGGCATTGAGGCTTGAG |
| *KCND2* | NM_019697 | $K_V4.2$ | CTGTGGTCACGTAAGGTTGT | GTGCAAGAACTCAGTACAATTCAG |
| *KCND3* | NM_001039347 | $K_V.4.3$ | ATCGAGCTCTCCATGCAG | CAAGACCACCTCACTCATCG |
| *KCNN1* | NM_032397 | $K_{Ca}2.1$ | CAAGCGGGTCAAAAATGCTG | GAAGGAACTTACGCTGGTGTTT |
| *KCNN2* | NM_080465 | $K_{Ca}2.2$ | AGCCGGAGCACAACAATTCTA | CCCAGCTTGTAGCCGATGT |
| *KCNN3* | NM_080466 | $K_{Ca}2.3$ | CTCGGAGAAACCTTATCGAGGC | GGTTGTGGGTAGCGTTGGG |
| *KCNMA1* | NM_010610 | $K_{Ca}1.1$ | CAGGCAGATGGTACTCTCAAGC | TTGGGTTTGACGAGTCTATGAAG |
| *SCN2A1* | NM_001099298 | $Na_v1.2$ | ACCAAGTTCTGAATAGCCCAA | CCAAATGTACTTCACCAATGCC |
| *SCN3A* | NM_001355166 | $Na_v1.3$ | CTTAGCCTTCTCTTCCTGACTTC | CAGCACCTTTGAAGATAGCGA |
| *SCN7A* | NM_009135 | $Na_v2.1$ | TCATGTCCGCATATTCCAGTAAG | GCTGGTTTGAGTGTTTCATTGG |
| *SCN8A* | NM_001077499 | $Na_v1.6$ | GTGACGAAATCAAAGACAATCCC | GACAGAGGAACAGAAGAAGTACTAC |
| *SCN9A* | NM_001290674 | $Na_v1.7$ | CTTCTGCCTCCTCTTCTCCT | GAGCTTAGCAGTGACTCAGATAG |
| *SCN1B* | NM_011322 | Navβ1 | GCACCTCATTCTCATAGCGTAG | CATCTCCTGTAAGCGTCGTAG |
| *SCNM1* | NM_027013 | $Na^+$ channel modifier | ATAGAAAAGCTTCAGACTGGACA | TGAGGACGAGGCACTGAT |

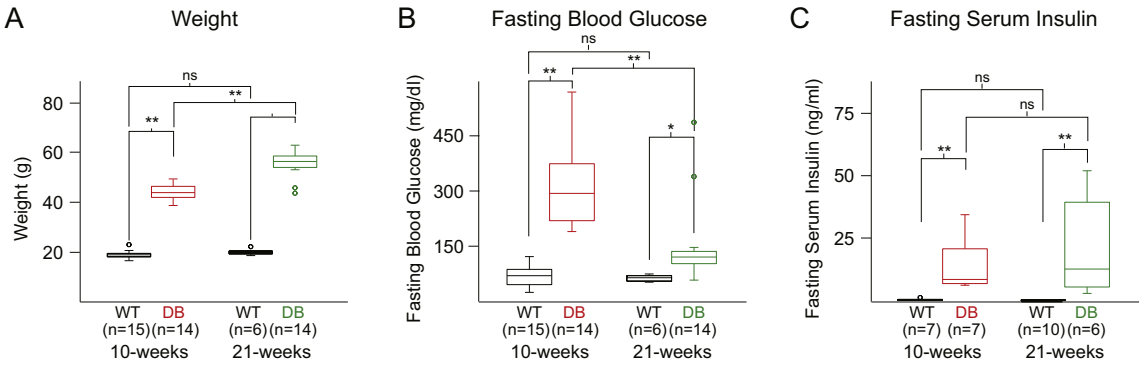


**Fig. 2.** Lepr$^{db/db}$ mice show a strong diabetic phenotype at week 10 with hyperglycemia that is somewhat reduced at week 21. Diabetes associated metabolic parameters of DB vs WT mice at different times; week 10 (*left*) or week 21 (*right*) in either wildtype (white) or diabetic conditions (red and green for weeks 10 and week 21 respectively). A. Diabetic Genotype significantly increased weight. Age increased weight in diabetic but not WT mice. B. Fasting blood glucose was significantly increased by diabetic condition, however, blood glucose went down with age within the diabetic condition. C. Fasting serum insulin was increased by diabetic condition but not by age. Holm-Sidak Post-Hoc test; *, $p < 0.05$; **, $p < 0.01$. (For interpretation of the references to color in this figure legend, the reader is referred to the web version of this article.)

**Table 2**
Diabetes associated metabolic parameters. Post hoc Holm-Sidak test: * $p < 0.05$ vs WT. ** $p < 0.05$ vs 9 week. n is number of animals.

| Property (unit) | Condition | Age (weeks) | (n) | Mean (SD) | ANOVA: F(df); (p =) | | |
|---|---|---|---|---|---|---|---|
| | | | | | Cond. | Age | Int. |
| Weight (g) | WT | 9 | 15 | 18.9 (1.6) | F(1,43) = 169.3; ($p < 10^{-8}$) | F(1,43) = 21.3; ($p < 3.5 \times 10^{-5}$) | F(1,43) = 3.4; (p = 0.072) |
| | | 21 | 6 | 20.0 (1.2) | | | |
| | DB | 9 | 13 | 44.0 (3.4)* | | | |
| | | 21 | 13 | 55.4 (5.5)*, ** | | | |
| Fasting Blood Glucose (mg/dl) | WT | 9 | 15 | 112.5 (27.1) | F(1,44) = 37.2 ($p = 2.4 \times 10^{-7}$) | F(1,44) = 8.9 (p = 0.005) | F(1,44) = 7.8 (p = 0.008) |
| | | 21 | 6 | 107.2 (8.7) | | | |
| | DB | 9 | 14 | 352.5 (115.2)* | | | |
| | | 21 | 13 | 196.6 (113.2)*, ** | | | |
| Fasting Serum Insulin (ng/ml) | WT | 9 | 7 | 0.5(0.4) | F(1,26) = 71.6 ($p < 10^{-8}$) | F(1,26) = 0.0 (p = 0.809) | F(1,26) = 0.0 (p = 0.916) |
| | | 21 | 6 | 0.3(0.1) | | | |
| | DB | 9 | 7 | 29.5(40.2)* | | | |
| | | 21 | 10 | 35.1(46.5))* | | | |

significantly heavier than WT at both time points (Fig. 2A, Table 2). In contrast, WT mice did not significantly differ in weight from weeks 10 to 21 (Fig. 2A, Table 2).

#### 3.2.1. Lepr$^{db/db}$ mice are hyperglycemic, especially when young

Surprisingly, in diabetic mice, fasting blood glucose (Fig. 2B) significantly decreased from week 10 to 21 (Fig. 2B, Table 2), this phenomena has been reported for C57BL/6J mice before, however, usually at later time points (~week 25–30; although still elevated compared to control (Gunnarsson, 1975)). Despite this, consistent with the diabetic phenotype, fasting blood glucose was significantly elevated in diabetic mice for both weeks 10 and 21 relative to control (Fig. 2B, Table 2). In contrast to diabetic mice, no significant difference was observed in the fasting blood glucose of WT mice between weeks 10 and 21 (Fig. 2B, Table 2).

#### 3.2.2. Lepr$^{db/db}$ mice have elevated plasma insulin

In C57BL/6J Lepr$^{db/db}$ mice the plasma insulin level is known to increase (Gunnarsson, 1975). Mean plasma insulin levels (Fig. 2C, Table 2) in diabetic mice were stable from week 10 to week 21, but were significantly elevated compared to WT, which also did not change from weeks 10 to 21 (Fig. 2C, Table 2). Together, these results support that the Lepr$^{db/db}$ manifests the insulin resistant, type II diabetic phenotype.

### 3.3. Passive properties of diabetic neurons change with age and diabetic condition

Data were collected from 115 neurons from 19 different animals; 38 neurons from 9, 10-week-old WT mice (WT10); 41 neurons from 5, 10-week-old diabetic mice (DB10); and 36 neurons from 5, 21-week-old diabetic mice (DB21). As we saw no significant difference in metabolic parameters for WT mice from weeks 10 to 21 (Fig. 2, Table 2), we assume WT physiology is likewise similar to WT21 (However, for caveats to this, see discussion below). Thus all WT recordings are made from 10-week old animals. In contrast to Tompkins et al. (2013) finding of depolarized RMP in diabetic animals, our data showed no difference in median RMP (Fig. 3A) between WT, DB10 or DB21 (Fig. 3A, Table 3). However, consistent with Tompkins et al. (2013) we found that median $R_{IN}$ (Fig. 3B, Table 3) was significantly reduced in DB21 but not in DB10 neurons, consistent with decreased excitability. We next estimated time constant by a 2-exponential fit (Golowasch et al., 2009; White and Hooper, 2013). Median time constant (Fig. 3C, Table 3), a parameter important in integration of synaptic inputs and firing pattern (Springer et al., 2015), showed a similar pattern, showing a significant reduction in DB21 but not DB10 when compared to WT neurons. Capacitance (Fig. 3D, Table 3) showed a different pattern, as DB10 but not DB21 was significantly increased relative to WT. Changes in capacitance could reflect a change in cell size or dendritic arbor (Golowasch et al., 2009), we suspect that since these cells typically have little to no dendrites (Jobling and Lim, 2008), the more parsimonious explanation would be an increase in neuron size in the DB10 condition. These data suggest that properties associated with excitability; $R_{IN}$ and time constant

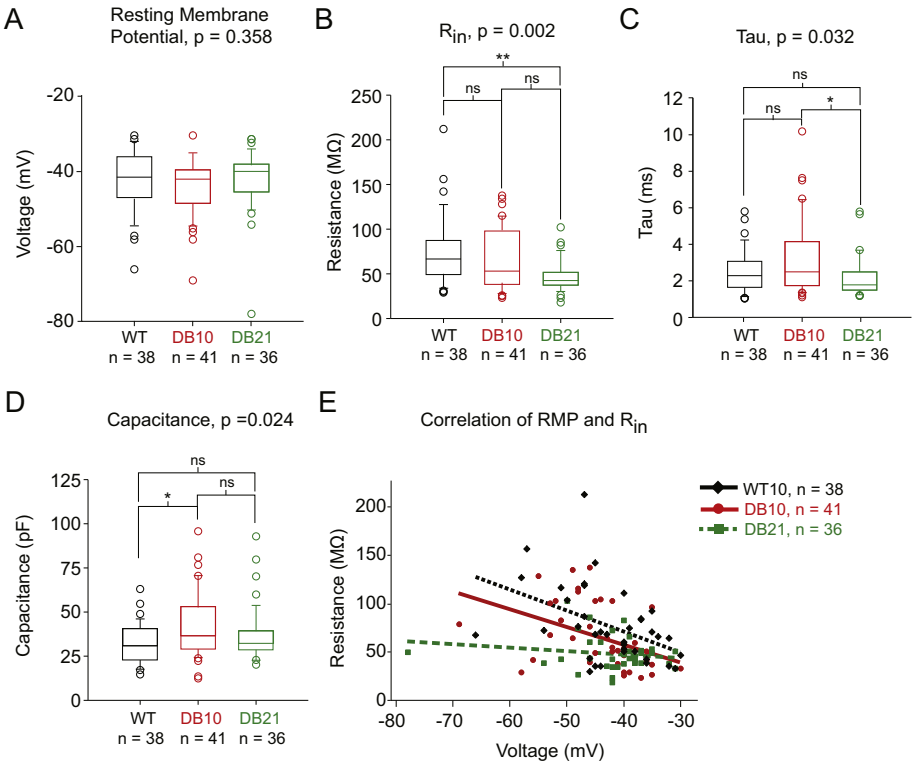


**Fig. 3.** Effect of condition for WT, DB10, and DB21 condition on passive properties of MPG neurons. A. RMP was not affected by diabetic condition. B. DB21 neurons showed reduced $R_{IN}$ compared to WT10. C. DB10 neuron $R_{IN}$ was significantly less than DB21 neurons. D. DB10 neurons showed significantly greater capacitance than WT10 neurons. Data shown are medians, quartiles and outliers. Dunn's test: * $p < 0.05$; **, $p < 0.01$. E. Correlation coefficient between RMP and $R_{IN}$ is altered by diabetic condition. Individual data points represent measurements of RMP and $R_{IN}$ from individual neurons. Fit lines represent correlation analyses via Pearson tests. $R_{IN}$ and RMP are significantly correlated in WT10 and DB10 but not DB21 conditions.

(Springer et al. 2015), are decreased in DB21 but not DB10, while capacitance is increased in 10-week diabetic female mice, but not at 21 weeks.

Impalement damage by sharp electrode recordings can depolarize RMP and reduce $R_{IN}$ (Li et al., 2004), and some studies try to correct for this by applying minimum $R_{IN}$ and RMP cut-offs (Springer et al., 2015; Tompkins et al., 2010; Tompkins et al., 2013). The MPG has a heterogenous population of neurons that vary in size (Keast, 1995, 2006), therefore, this method of arbitrary cut offs, especially for input resistance, are inappropriate, especially when differences in conditions are unknown. Therefore, we tried and failed to create a uniform empirical cut off for inclusion criteria. We initially reasoned that if RMP and $R_{IN}$ are predictors of cell health, we should see a correlation between the two, that should weaken as these cut offs became more stringent and only undamaged cells remained. While applying RMP cut offs from −25 mV to −40 mV did not weaken this correlation, we did observe something more interesting. As illustrated in Fig. 3E, there is a significant correlation between $R_{IN}$ and RMP in WT10 and DB10 conditions, although these correlations are weaker in DB10 animals than WT (Pearson correlation tests, WT: $r = -0.562$, $p < 8.62 \times 10^{-4}$; n = 31; DB10: $r = -0.376$, $p = 0.008$; n = 48). However, DB21 lost the correlation between $R_{IN}$ and RMP altogether ($r = -0.170$, $p = 0.323$, n = 36). This change in correlation suggests that the diabetic condition itself reduces the validity of $R_{IN}$ and RMP as uniform predictors of cell health. In other words, the DB21 condition is confounded with cut offs for $R_{IN}$. Since uniform inclusion criteria could not be applied across groups without bias, we decided to be as permissive as possible to facilitate comparisons between conditions as described in the methods. While this approach runs the risk of including more cells that could be deemed "unhealthy" in the data set, there is no reason to suspect that cell health or impalement damage would not be uniform across groups. Thus an objective and inclusive comparison of data across groups allows for us to determine how diabetes *changes* cell properties in an unbiased manner – even if the population data may lack some biological accuracy with regard to absolute membrane potential.

**Table 3**
Effect of diabetic condition on passive properties of MPG neurons. n is number of neurons.

| Property (unit) | Condition | Age (weeks) | (n) | Mdn. | 75th per. | 25th per. | KW ANOVA: H(df); (p =) |
|---|---|---|---|---|---|---|---|
| RMP (mV) | WT | 10 | 37 | −43.0 | −36.5 | −47.0 | H(2) = 2.02 |
| | DB | 10 | 41 | −42.0 | −39.5 | −48.5 | p = 0.365 |
| | DB | 21 | 36 | −40.0 | −38.0 | −45.5 | |
| $R_{in}$ (MΩ) | WT | 10 | 37 | 68.0 | 89.0 | 44.0 | H(2) = 10.6 |
| | DB | 10 | 41 | 51.0 | 89.0 | 38.0 | p = 0.005 |
| | DB | 21 | 36 | 42.5* | 51.8 | 37.3 | |
| Time constant (ms) | WT | 10 | 37 | 2.3 | 3.2 | 1.6 | H(2) = 6.81 |
| | DB | 10 | 41 | 2.5 | 4.2 | 1.7 | p = 0.033 |
| | DB | 21 | 36 | 1.8 | 2.5 | 1.5 | |
| Capacitance (pF) | WT | 10 | 37 | 33.8 | 41.0 | 29.8 | H(2) = 23.19 |
| | DB | 10 | 41 | 48.7* | 57.8 | 39.6 | p < 0.001 |
| | DB | 21 | 36 | 41.9* | 54.8 | 35.1 | |

* $p < 0.05$ vs WT10 (Dunn's method).

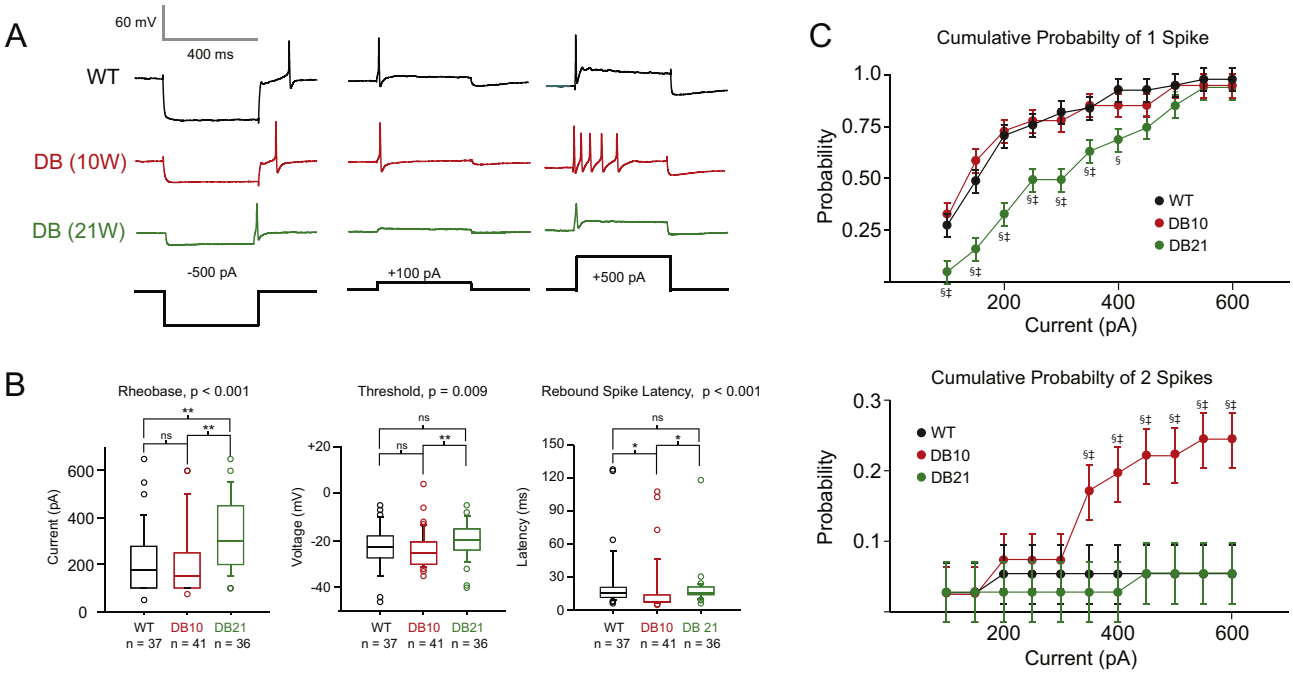


**Fig. 4.** DB10 and DB21 conditions increase and decrease excitability of MPG neurons, respectively. A. Representative traces of intracellular currents injections of −500 pA, 100 pA and 500 pA current injections in WT10 (black), DB10 (red) or DB21 (green). B. *Left:* Rheobase was significantly altered by diabetic condition. *Center:* Threshold (Fig. 1, 12) was significantly altered by diabetic condition. *Right:* Diabetic condition significantly altered latency to first rebound spike. Shown are Medians, quartiles and outliers. Dunn's test;*, $p < 0.05$; **, $p < 0.01$. ***, $p < 0.001$. C. *Top:* Two-way ANOVA for factors current and condition showed that cumulative probability of firing 1 or more spikes as a function of injected current was reduced in DB21 condition [Condition; $F(2, 1443) = 37.997$ $p < 1 \times 10^{-8}$. Current; $F(12, 1443) = 51.817$, $p < 1 \times 10^{-8}$. Interaction; $F(24, 1443) = 2.038$, $p = 0.002$.]. *Bottom:* A two-way ANOVA showed that the Cumulative probability of firing 2 or more spikes as a function of injected current was increased in the DB10 condition [Condition; $F(2, 1443) = 43.428$, $p < 1 \times 10^{-8}$. Current; $F(12, 1443) = 2.251$, $p = 0.008$. Interaction; $F(24, 1443) = 1.301$, $p = 0.150$.]. Note difference in scale. Holm-Sidak post hoc tests: $p < 0.05$; * WT10 vs DB10, † WT10 vs DB21,‡ DB10 vs DB21. Shown are Means ± SEM. (For interpretation of the references to color in this figure legend, the reader is referred to the web version of this article.)

### *3.4. Firing properties of Lepr$^{db/db}$ neurons changes with diabetic condition and time*

#### *3.4.1. DB10 and DB21 neurons have enhanced and reduced excitability, respectively*

Our hypothesis was that since diabetes causes diabetic cystopathy (Kebapci et al., 2007) and other lower intestinal symptoms (Vinik et al., 2003), presumably, at least in part through diabetic autonomic dysregulation (Nadelhaft and Vera, 1992); Lepr$^{db/db}$ efferent neurons of the MPG may contribute to these pathological changes and manifest themselves as changes in intrinsic excitability. Therefore, we first examined whether MPG neurons from different diabetic conditions would spike differently in response to depolarizing current steps from 0 to +700 pA in 50 pA increments (Fig. 4A, Table 4).

The representative neurons in Fig. 4A show that DB10 (Red) neurons appear to be more excitable than WT (Black). In contrast, DB21 neurons (Green) were less excitable than either DB10 or DB21, and consistent with our finding of reduced $R_{IN}$ in these animals. Surprisingly, across all conditions, of the 115 neurons studied, only 13 (11.3%) produced more than one spike at any current injection level. Of the neurons that spiked more than once, 76.9% (10/13) were in the DB10 condition compared to a 15.4% (2/13) and 7.7% (1/13) contribution from WT and DB21 groups respectively.

The probability of finding a neuron spiking more than once was 5.4% (2/37), 24.4% (10/41) and 2.8% (1/36) for WT, DB10 and DB21 groups respectively. This is lower than was expected for WT mice as multispiking cells was reported to be about 28.6% in female C57BL/6J mice previously (Jobling and Lim, 2008). A Chi square test showed that group as a factor was not statistically independent ($X^2$ (2, N = 114) = 8.268, p = 0.016) suggesting that diabetic condition altered max number of spikes. Similarly; a Kruskal-Wallis test showed these groups were significantly different, however, this test is more dubious as all groups had median = 1 (Table 4). Due to this low spike probability, we could not run more conventional IO curves. Therefore, instead of IO curves, we examined the cumulative probability of producing one or more spikes as a function of current injected. Cumulative probability of firing 1 or more spikes as a function of injected current was reduced in DB21 condition but was not significantly different between DB10 and WT neurons (Fig. 4C, Top). Unfortunately, this particular distribution was neither normally distributed nor homoscedastic due to its binary nature. Supporting the reduced excitability of DB21 neurons was the finding that median rheobase was increased in DB21 relative to WT and DB10 (Fig. 4B, Left; Table 4). Together, these data support DB21 mice having reduced MPG excitability.

#### *3.4.2. DB10 condition enhances excitability*

When examining the probability of these neurons firing twice or more, neurons from DB10 had significantly greater probability of firing more than two spikes compared to both WT and DB21 (Fig. 4C, Bottom; Table 4). Median DB10 rheobase was not significantly different from WT, but was significantly less compared to DB21 (Fig. 4B, Left; Table 4.). In agreement with this, DB10 threshold was hyperpolarized compared to DB21 (Fig. 4B, Center; Table 4), however, it was not significantly different from WT. These results, suggest that DB10 excitability is enhanced relative to WT and DB21 conditions.

#### *3.4.3. Rebound spike latency is decreased in DB10 neurons*

90.4% (104/115) of cells healthy enough for inclusion, produced rebound spikes in response to release of hyperpolarizing current injection (anode break excitation). This is consistent with previous

**Table 4**
Effect of diabetic condition on excitability properties of MPG neurons. n is number of neurons.

| Property (unit) | Condition | Age (weeks) | (n) | Mdn. | 75th per. | 25th per. | KW ANOVA: H(df); (p =) |
|---|---|---|---|---|---|---|---|
| Rheobase (pA) | WT | 10 | 37 | 150 | 275 | 100 | H(2) = 16.05 |
| | DB | 10 | 41 | 150 | 250 | 100 | p < 0.001 |
| | DB | 21 | 36 | 300* | 450 | 200 | |
| Threshold (mV) | WT | 10 | 37 | −22.0 | −18.0 | −27.5 | H(2) = 9.35 |
| | DB | 10 | 41 | −25.0 | −20.5 | −30.0 | p = 0.009 |
| | DB | 21 | 36 | −19.5 | −15.0 | −24.0 | |
| Rebound Spike Latency (ms) | WT | 10 | 35 | 15.4 | 20.9 | 11.5 | H(2) = 22.90 |
| | DB | 10 | 34 | 7.9* | 13.9 | 7.1 | p < 0.001 |
| | DB | 21 | 33 | 15.7 | 21.2 | 14.1 | |
| Spike latency at Rheobase (ms) | WT | 10 | 37 | 14.1 | 17.8 | 10.8 | H(2) = 0.464 |
| | DB | 10 | 41 | 13.9 | 17.6 | 12.2 | p = 0.793 |
| | DB | 21 | 36 | 15.3 | 18.3 | 11.7 | |
| Max Spikes (spikes) | WT | 10 | 37 | 1.0 | 1.0 | 1.0 | H(2) = 10.83 |
| | DB | 10 | 41 | 1.0 | 1.5 | 1.0 | p = 0.004 |
| | DB | 21 | 36 | 1.0 | 1.0 | 1.0 | |

* $p < 0.05$ vs WT10 (Dunn's method).

reports that the majority of intact male rat MPG neurons produce rebound spikes (Tan et al. 2007), despite dissociated neuron studies showing a sharp divide where sympathetic neurons produce copious rebound spikes while parasympathetic neurons produce none (Lee et al., 2002). Therefore, another sign of increased excitability was that latency to first spike after release of hyperpolarizing current injection (Right, Fig. 4B) was significantly decreased in the DB10 condition compared to WT and DB21 conditions (Fig. 4B, Right; Table 4). These data support excitability being enhanced in the DB10 condition.

### 3.4.4. Ascending spike slope is increased in response to depolarizing current injection in the DB10 condition but not first rebound spike

To establish how observed changes in excitability caused by diabetic condition occurred, we examined whether diabetic condition and age modulated properties of the action potentials (illustrated in Fig. 1). Fig. 5A1 shows representative samples of action potential waveforms observed in diabetic conditions for a *rebound* spike. Note that most prominently, AP latency is decreased in DB10 condition relative to WT10 and DB21. The derivative plot of these samples in Fig. 5A2 reveals that both maximum and minimum AP slope ($\frac{dv}{dt}$), and AHP height appear to be altered by diabetic condition. However, when quantified, only descending slope was shown to be significantly altered in DB10 *rebound* spikes. While we did see that the ascending action potential slope in response to *depolarizing* current injections was increased in DB10 mice (Fig. 5B, Table 5), when *rebound* spikes were examined, this trend was *not* supported. This is because neither median maximum ascending slope nor 10–90% rise slope (Fig. 1, 7), were significantly enhanced in DB10 condition (Fig. 5D, H; Table 5). We believe this difference was real and not due to a reduction in statistical power, as within WT groups, the coefficient of variance in ascending slope for depolarizing current injections was greater (CV = 1.14) than for *rebound* spikes (CV = 0.79). For *rebound* spikes, as the peak ascending slope of the AP did not increase, we suspect the sum of inward and outward currents did not increase. In contrast, for spikes initiated by *depolarization*, the maximum slope was increased in the diabetic condition, suggesting that net membrane current is more inward during the upstroke of the action potential. The most parsimonious explanation for this observation would be a change to sodium channels of the same conductance with a more depolarized $V_{1/2}$ inactivation in the DB10 condition, but more voltage clamp and pharmacological work is needed due to the limitations of current clamp (see discussion) .

____'

### 3.4.5. AP half-width is decreased while decay slope is increased in rebound spikes of DB10 neurons

In contrast to ascending slope in rebound spikes that did not change in DB10, we found that the median width of the action potential at half its maximal height (i.e. half-width; Fig. 1, 3) was significantly reduced in the DB10 condition compared to DB21 but not vs WT (Fig. 5E, Table 5).

Part of the reduction in DB10 half-width may be explained by the finding that that both maximal and 90–10% decay slope increased (Also see discussion). This is shown as median maximal decay slope was made more negative (increased) in DB10 neurons vs DB21 neurons but not vs WT neurons suggesting these neurons repolarized faster (Fig. 5E, Table 5). In agreement with this, median 90–10% decay slope also became more negative in the DB10 condition vs WT and compared to DB21 (Fig. 5I, Table 5). Accordingly, median 90–10% decay time significantly decreased in DB10 vs WT and DB21 (Fig. 5G, Table 5). These data, in combination with the finding that AP ascending slope did not increase in rebound spikes, suggests that AP half-width decreased primarily through a mechanism that increases AP descending slope. This increase in AP descending slope also suggests an increase in the sum of currents during the downstroke of the AP. We suggest that the most parsimonious explanation would be an increase in outward currents, but caveat that further voltage clamp and pharmacological work is required (see discussion).

### 3.4.6. AP area and AHP decay constant decreased in DB10 with no changes in after hyperpolarization (AHP) area

Consistent with decreased AP half-width, total AP area (excluding the AHP) was significantly decreased in DB10 neurons relative to DB21 but not when compared to WT (Fig. 5J, Table 5). This was not due to changes in spike height, as neither DB10 nor DB21 differed significantly in spike height relative to WT (Table 5). If AP area decreased, a possible mechanism would be activation of outward currents, and one might expect to see an enhanced AHP. However, surprisingly, no change in AHP area for DB10, nor DB21 vs WT, were observed (Fig. 5K, Table 5). Neither were changes observed in AHP height (Fig. 1, 2) in DB21, DB10 conditions vs WT (Fig. 5L, Table 5). Despite our finding of stable AHP amplitude and area, we did see that AHP decay tau significantly decreased in DB10 neurons vs WT and DB21 neurons (Fig. 5M, Table 6). Although this change in minimum AP slope would suggest that total membrane current is increasing in the outward direction during repolarization, the lack of increased AHP height would suggest that, if this is due to a shift in potassium currents, it would be to those with faster deactivation times; since faster deactivating potassium currents with more depolarized half activations enable faster spiking (Boddum et al. 2017; Rudy and McBain, 2001), this would be consistent with our observations of increased multispikers in the DB10 condition (see discussion below). These data, along with our finding of increased decay slope suggest that DB10 condition is repolarizing faster than other

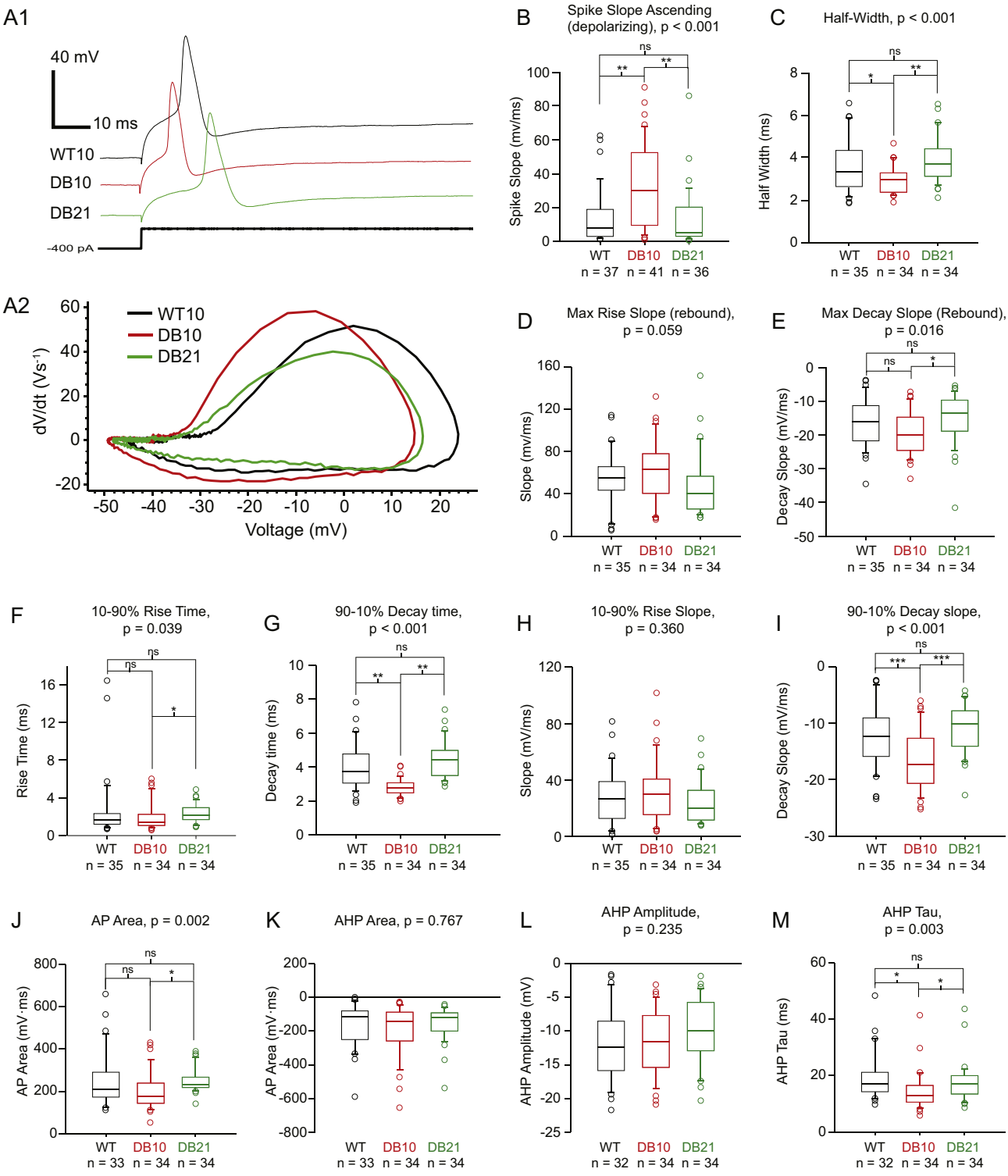


**Fig. 5.** Action potential (AP) parameters are altered by DB condition in mouse MPG neurons. All data except B were quantified from rebound spikes. A1. Representative samples of rebound spikes from WT10, DB10, and DB21 groups. A2. Derivative plot of action potentials shown in A1. Note that rebound latency, spike width, and max decay slope (maximum negative dv/dt) were significantly decreased in DB10 condition. B. In response to depolarizing current injections, DB10 neurons had significantly increased ascending spike slope (1). C. Rebound spikes in DB10 neurons had significantly reduced AP half-width (3). D. Diabetic condition did not significantly alter AP maximum rise slope (10). E. DB10 neurons appeared to have more negative maximum AP decay slope (11). F. DB10 neurons appeared to have reduced AP 10-90% rise time (4). G. DB10 neurons had significantly reduced 90-10% decay time (5). H. Diabetic condition had no effect on 10-90% AP rise slope (7). I. DB10 neurons had more negative 90-10% decay slopes (8). J. DB10 neurons had reduced AP area (6). K. Diabetic condition did not did not alter AHP area (13). L. Diabetic condition did not alter AHP amplitude (2). M. DB10 had significantly reduced AHP decay tau (14). Data shown are medians, quartiles, and outliers. Dunn's test: * $p < 0.05$; ** $P < 0.01$.

**Table 5**
Effect of diabetic condition on Action Potential properties of MPG neurons. n is number of neurons.

| Property (unit) | Condition | Age (weeks) | (n) | Mdn. | 75th per. | 25th per. | KW ANOVA: H(df); (p =) |
|---|---|---|---|---|---|---|---|
| Ascending spike Slope (depolarizing current; mV/ms) | WT | 10 | 37 | 8.0 | 19.0 | 3.3 | H(2) = 22.01 |
| | DB | 10 | 41 | 30.0* | 52.5 | 9.5 | p < 0.001 |
| | DB | 21 | 36 | 5.0 | 20.3 | 3.0 | |
| AP Half-Width (ms) | WT | 10 | 35 | 3.3 | 4.4 | 2.6 | H(2) = 14.89 |
| | DB | 10 | 34 | 3.0* | 3.3 | 2.4 | p < 0.001 |
| | DB | 21 | 34 | 3.7 | 4.4 | 3.1 | |
| Max Rise Slope (mV/ms) | WT | 10 | 35 | 55.3 | 66.2 | 43.1 | H(2) = 5.67 |
| | DB | 10 | 34 | 62.8 | 77.9 | 40.3 | p = 0.059 |
| | DB | 21 | 34 | 40.3 | 56.6 | 25.6 | |
| Max Decay Slope (mV/ms) | WT | 10 | 35 | −15.9 | −11.3 | −21.7 | H(2) = 8.11 |
| | DB | 10 | 34 | −20.0 | −14.7 | −24.6 | p = 0.017 |
| | DB | 21 | 34 | −13.4 | −9.7 | −18.9 | |
| 10–90% Rise Time (ms) | WT | 10 | 35 | 1.6 | 2.4 | 1.2 | H(2) = 6.46 |
| | DB | 10 | 34 | 1.4 | 2.3 | 1.1 | p = 0.039 |
| | DB | 21 | 34 | 2.1 | 3.0 | 1.7 | |
| 90–10% Decay Time (ms) | WT | 10 | 35 | 3.7 | 4.8 | 3.0 | H(2) = 42.20 |
| | DB | 10 | 34 | 2.7* | 3.1 | 2.5 | p < 0.001 |
| | DB | 21 | 34 | 4.4 | 5.0 | 3.5 | |
| 10–90% Rise Slope (mV/ms) | WT | 10 | 35 | 25.8 | 39.5 | 12.4 | H(2) = 2.04 |
| | DB | 10 | 34 | 29.8 | 40.6 | 15.4 | p = 0.360 |
| | DB | 21 | 34 | 20.0 | 32.7 | 11.5 | |
| 90–10% Decay Slope (mV/ms) | WT | 10 | 35 | −12.6 | −9.0 | −15.9 | H(2) = 18.86 |
| | DB | 10 | 34 | −17.4* | −12.7 | −20.7 | p < 0.001 |
| | DB | 21 | 34 | −10.1 | −7.8 | −14.1 | |
| AP Area (mV·ms) | WT | 10 | 33 | 209.8 | 290.7 | 172.0 | H(2) = 12.32 |
| | DB | 10 | 34 | 174.4 | 238.8 | 142.7 | p = 0.002 |
| | DB | 21 | 34 | 232.5 | 266.7 | 217.5 | |
| AP Height (mV) | WT | 10 | 37 | 64.5 | 80.1 | 52.7 | H(2) = 0.498 |
| | DB | 10 | 41 | 63.6 | 78.1 | 37.9 | p = 0.779 |
| | DB | 21 | 36 | 61.2 | 75.9 | 53.8 | |
| Baseline slope (mV/ms)† | WT | 10 | 35 | −0.3 | −0.2 | −0.5 | H(2) = 1.72 |
| | DB | 10 | 34 | −0.3 | −0.1 | −0.4 | p = 0.424 |
| | DB | 21 | 34 | −0.2 | −0.1 | −0.1 | |
| Baseline‡ | WT | 10 | 35 | −40.3 | −36.5 | −46.6 | H(2) = 2.34 |
| | DB | 10 | 34 | −39.7 | −35.8 | −45.4 | p = 0.310 |
| | DB | 21 | 34 | −38.5 | −35.3 | −41.4 | |
| AP Mean Height, (mV)†‡ | WT | 10 | 35 | 2.4 | 3.3 | 0.5 | H(2) = 8.29 |
| | DB | 10 | 34 | 0.5* | 2.2 | −0.7 | p = 0.016 |
| | DB | 21 | 34 | 1.7 | 2.7 | 0.6 | |

* p < 0.05 vs WT10 (Dunn's method).
† Internal control that is best fit line to sampled interval.
‡ RMP during rebound spike.
†‡ Mean of sampled interval during rebound spike.

conditions. Surprisingly, diabetic condition and age interact to alter AP area and AHP decay constant while leaving other AP parameters unmodified.

### 3.4.7. 2nd AHPs and ADPs after 145 ms

When quantifying properties of the AHP, it was found that after the initial AHP, some neurons had after depolarizations, while some had secondary slower AHPs and still others had both. We attempted to systematically quantify this across conditions by analyzing the change

**Table 6**
Effect of diabetic condition on after hyperpolarization and other properties of MPG neurons. n is number of neurons.

| Property (unit) | Condition | Age (weeks) | (n) | Mdn. | 75th per. | 25th per. | KW ANOVA: H(df); (p =) |
|---|---|---|---|---|---|---|---|
| AHP Area (mV·ms) | WT | 10 | 33 | −116.6 | −80.6 | −251.1 | H(2) = 0.530 |
| | DB | 10 | 34 | −141.6 | −88.1 | −259.2 | p = 0.767 |
| | DB | 21 | 34 | −121.9 | −92.1 | −200.5 | |
| AHP amplitude (mV) | WT | 10 | 32 | −12.4 | −8.5 | −15.9 | H(2) = 2.90 |
| | DB | 10 | 34 | −11.6 | −7.7 | −15.4 | p = 0.235 |
| | DB | 21 | 34 | −10.0 | −5.8 | −12.9 | |
| AHP Tau (ms) | WT | 10 | 32 | 16.9 | 21.2 | 14.2 | H(2) = 11.90 |
| | DB | 10 | 34 | 13.0* | 16.5 | 10.5 | p = 0.003 |
| | DB | 21 | 34 | 17.0 | 20.0 | 13.4 | |
| Time (AP to AHP peak; ms) | WT | 10 | 35 | 8.3 | 11.0 | 7.3 | H(2) = 31.9 |
| | DB | 10 | 34 | 6.9* | 7.5 | 6.1 | p < 0.001 |
| | DB | 21 | 34 | 9.8 | 11.2 | 8.1 | |
| ΔV 145 ms after AP repolarization (mV) | WT | 10 | 22 | 2.6 | 4.0 | 1.3 | H(2) = 14.33 |
| | DB | 10 | 15 | 2.0 | 2.0 | 0.9 | p < 0.001 |
| | DB | 21 | 32 | 1.0* | 1.8 | 0.2 | |

* p < 0.05 vs WT10 (Dunn's method).

in voltage 145 ms after the descending stroke of the AP recrossed baseline. However, this comes with the caveat that some neurons could not be quantified due to no change in baseline (ambiguous AHP or RMP drift), multiple rebound spikes, or loss of cells. Within 73.0% (27/37) of quantified WT neurons, 81.5% (22/27) displayed afterdepolarizations, while the remaining 18.5% (5/27) displayed secondary after hyperpolarizations and none displayed both. Within DB10 neurons 4.9% (2/41) could not be classified due to multiple rebound spikes. However, of the 82.9% (34/41) that could be quantified, 44.1% (15/34) showed ADPs, 20.6% (7/34) showed secondary AHPs; in contrast to WT; where 29.4% (10/34) of these neurons showed both AHPs and ADPs. Within 94.4% (34/36) of quantified DB21 neurons, 76.5% (26/34) showed ADPs, 2.9% (1/34) showed secondary AHPs, while 20.6% (7/34) showed both. A Chi Square test showed that these groups were not statistically independent ($X^2$ (4, N = 95) = 15.960, p = 0.003). Alternatively, when we just quantified the absolute voltage change at 145 ms, DB10 but not DB21 neurons were significantly different from WT neurons (Table 6). These data suggest that the DB10 condition is more likely to have slow AHPs or a lack of ADPs relative to WT.

### 3.5. Ion channels show widespread changes in expression in both DB10 and DB21 animals

We specifically focused on subsets of ion channel genes for this study to start to understand the underlying mechanisms for changes in excitability that we detected in MPG neurons of diabetic animals. The genes of interest are described in Table 1, including the currents to which each are known to contribute. We sampled alpha subunits for voltage-dependent $Ca^{2+}$ channels (*CACNA1A-H),* a subset of $Na^+$ channels (*SCNx*), and six families of $K^+$ channels (*KCNA, KCNB, KCNC, KCND, KCNN, KCNMA*). *CACNA1B, SCN8A,* and *KCNC1* were below our threshold of detection and may not be expressed in MPG neurons. Of the 30 other ion channel genes studied, 8 were significantly different between DB10 and control wild-type animals (Fig. 6). The voltage-dependent $Ca^{2+}$ channels *CACNA1A*, *CACNA1E* and *CACNA1H* were significantly higher in DB10 animals relative to control. The only $Na^+$ channel gene that was changed was a significant increase in *SCN2A1* in DB10 animals. In addition, 4 $K^+$ channel genes showed altered expression in DB10 animals: *KCNA3* was significantly lower in DB10 animals, while *KCNB1, KCNC2,* and *KCND3* were significantly higher in DB10 mice.

In DB21 animals, 12 channel genes showed differential expression relative to wild-type controls (Fig. 6). *CACNA1D* and *CACNA1G* were significantly higher in DB21 animals relative to control. There were no significant differences in sodium channel gene expression seen between DB21 and wild-type animals. However, there were 10 different $K^+$ channel genes that showed changes in expression in DB21 animals. *KCNA2, KCNA3, KCNA5,* and *KCNC3* were all significantly lower in DB21 animals than wild-type, with *KCNA2* and *KCNC3* expression all but abolished in the DB21 animals. *KCNC4, KCND2, KCND3, KCNN1, KCNN3* and *KCNMA1* were all significantly higher in DB21, with *KCND2* expression only detectable in DB21 animals. Most of these changes are seen only in DB21 animals and not in DB10, including *KCNA2, KCNA5 KCNC3, KCNC4, KCND2, KCNN1, KCNN3* and *KCNMA1*.

Some changes seen in DB10 animals resolved to control levels in the DB21 animals, while others persisted throughout the DB21 time point (Fig. 6). *KCNA3* was significantly lower in DB10 animals, and this change persisted into the DB21 group. *KCND3* was significantly increased in both DB10 and DB21 animals. Conversely, *KCNB1* was significantly higher in the DB10 animals, but returned to control levels in DB21 animals. Finally, there were some channels that were significantly different only between DB10 and DB21. *KCNA1* and *KCND1* were significantly higher in DB21 than DB10, although there was a trend towards these two channels being downregulated in DB10 overall, even though this did not reach statistical significance relative to control. The converse was true for *KCNB2*, which was significantly higher in DB10 than DB21 – although there was a trend for this channel to be transiently upregulated in the DB10 group.

### 3.6. Principal components analysis to further examine differences among groups in firing properties and channel expression

We next used principal component analysis (PCA) to visualize potential patterns and correlations in the features that may underlie distinctions in both the spike properties and channel expression across groups. A variance plot of the first two principal components (PC) for spike characteristics (Fig. 7A) demonstrates that there is overlapping features in all three groups that do not distinguish these groups in any obvious way. There is one major PC (PC1) that accounts for the majority of the variance in the data 42.5%, Fig. 7B). The variables that most contribute to the variance in spike characteristics largely consist of features involved in shaping the action potential dynamics underlying spike shape, such as decay slope, rise slope, and the amplitude of the spike (e.g. spike height, peak amplitude). These would be consistent with changes in $Na^+$ and $K^+$ channel expression, particularly those subtypes involved in the spiking itself. However, there is no combination of features that separates the diabetic animals from the wild-types, or each other, in a discrete fashion.

The PCA for channel expression in the MPG tells a different story. The variance plot of PC1 and PC2 (Fig. 8A) shows clear separation of all three groups, and the scree plot (Fig. 8B) shows that these two PCs account for the majority of the variance in the data. When looking at the channels that contribute to PC1 and PC2, it is also clear validation of the changes in expression reported in Fig. 6. By examining the vector plot in Fig. 8A and the contributions to PC1 in Fig. 8B, it is possible to discriminate a group of channels largely responsible for distinguishing the DB21 animals. The top ten contributors to PC1 consists entirely of channels that are uniquely and differentially expressed in DB21 animals relative to both DB10 and control. Conversely, by examining the top ten contributors to PC2 – in conjunction with the vector plot – it can be seen that PC2 consists of channels uniquely and differentially expressed in DB10 animals (*CACNA1A, CACNA1E, SCN2A1, KCNB1, KCNC2*) as well as channels that are both changed in the same direction in DB10 and DB21 (*KCND3*).

## 4. Discussion

Diabetic cystopathy has formally been documented since 1864 (Faerman et al., 1971), yet the only direct attempt to document how diabetes impacts efferent MPG neurons was by Tompkins et al. (2013), who focused largely on synaptic properties. Therefore, in this study we attempted to identify for the first time the impacts of a type II diabetes model on the intrinsic properties of MPG neurons in female mice. We hypothesized that passive properties, overall excitability and action potential properties in MPG neurons would change in an age-dependent manner within the diabetic condition. Furthermore, we examined underlying changes in mRNA levels for voltage-dependent ion channels in the whole ganglion as a reflection of the most salient of changes in excitability and firing of MPG neurons.

Lepr $^{db/db}$ mice on the C57BL/6J strain used here model hyperglycemia and persistent hyperinsulinemia with beta cell hypertrophy, whereas those on the BKS background strain progress to beta cell failure (Hummel et al., 1972). Although the mice in this study were diabetic at both ages, their hyperglycemia was somewhat worse at 10 weeks than at 21 weeks, consistent with previous observations in this strain (Breyer et al., 2005; Sullivan et al., 2007). This improvement was consistent with the constant serum insulin concentrations at 21 weeks, indicating that while the beta cells are not able to adequately compensate for insulin resistance, they have not undergone beta cell failure.

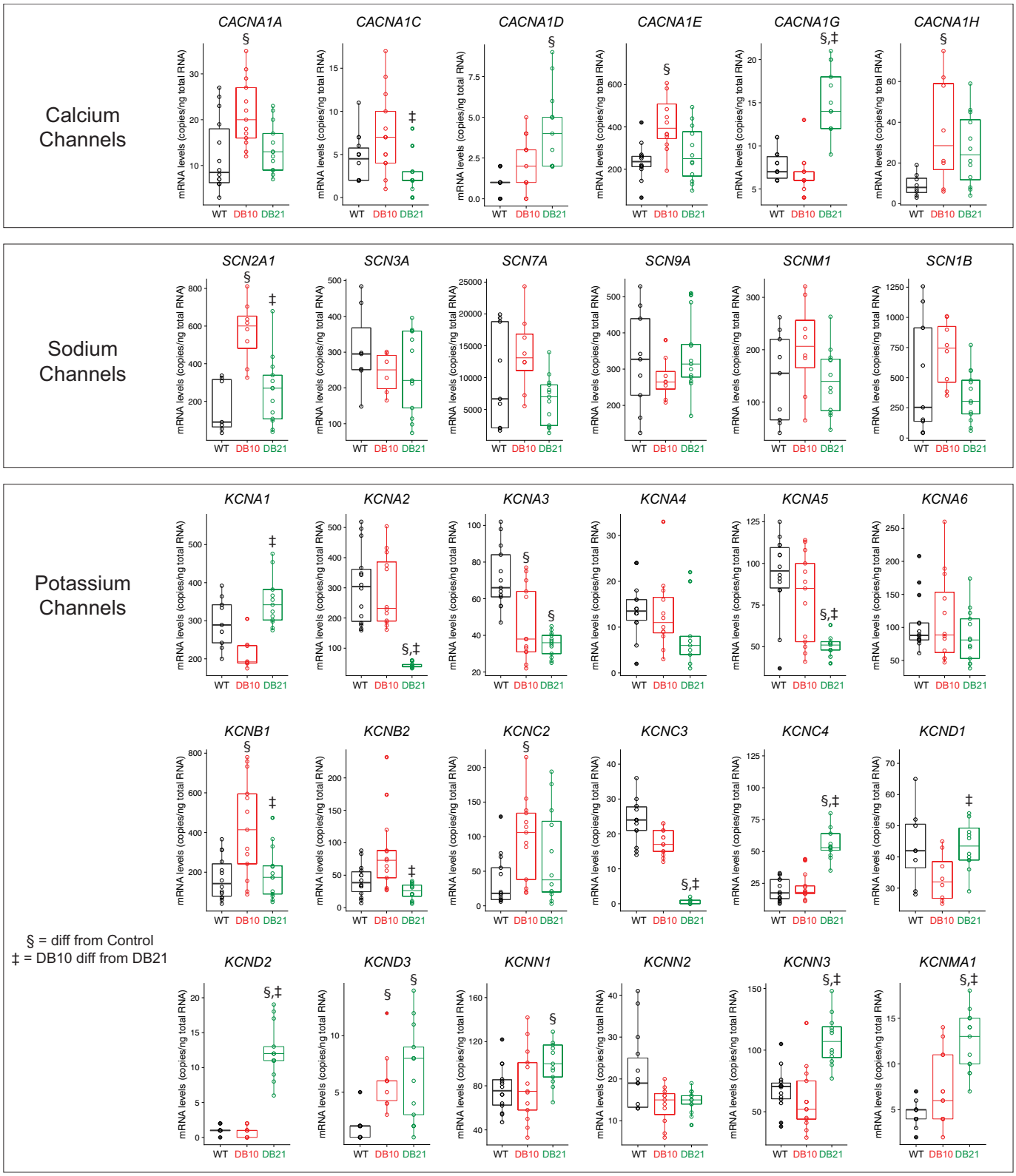


**Fig. 6.** mRNA copy numbers for ion channel subunits of across WT, DB10, and DB21 experimental groups. Significant differences as noted ($p < 0.05$; post-hoc Holm-Šídák analyses following One-Way ANOVA) represent pairwise comparisons across all three groups. Data shown are medians, quartiles and each individual value from a given animal.

### *4.1. Diabetes interacts with time to first increase then decrease MPG neuron excitability*

One of our most important findings was that excitability of MPG neurons in Lepr$^{db/db}$ females changes nonlinearly with the amount of time exposed to the diabetic environment. Specifically, we observed that 10 week Lepr$^{db/db}$ mice had an increased probability of firing two or more spikes, and decreased rebound spike latency; both of which are

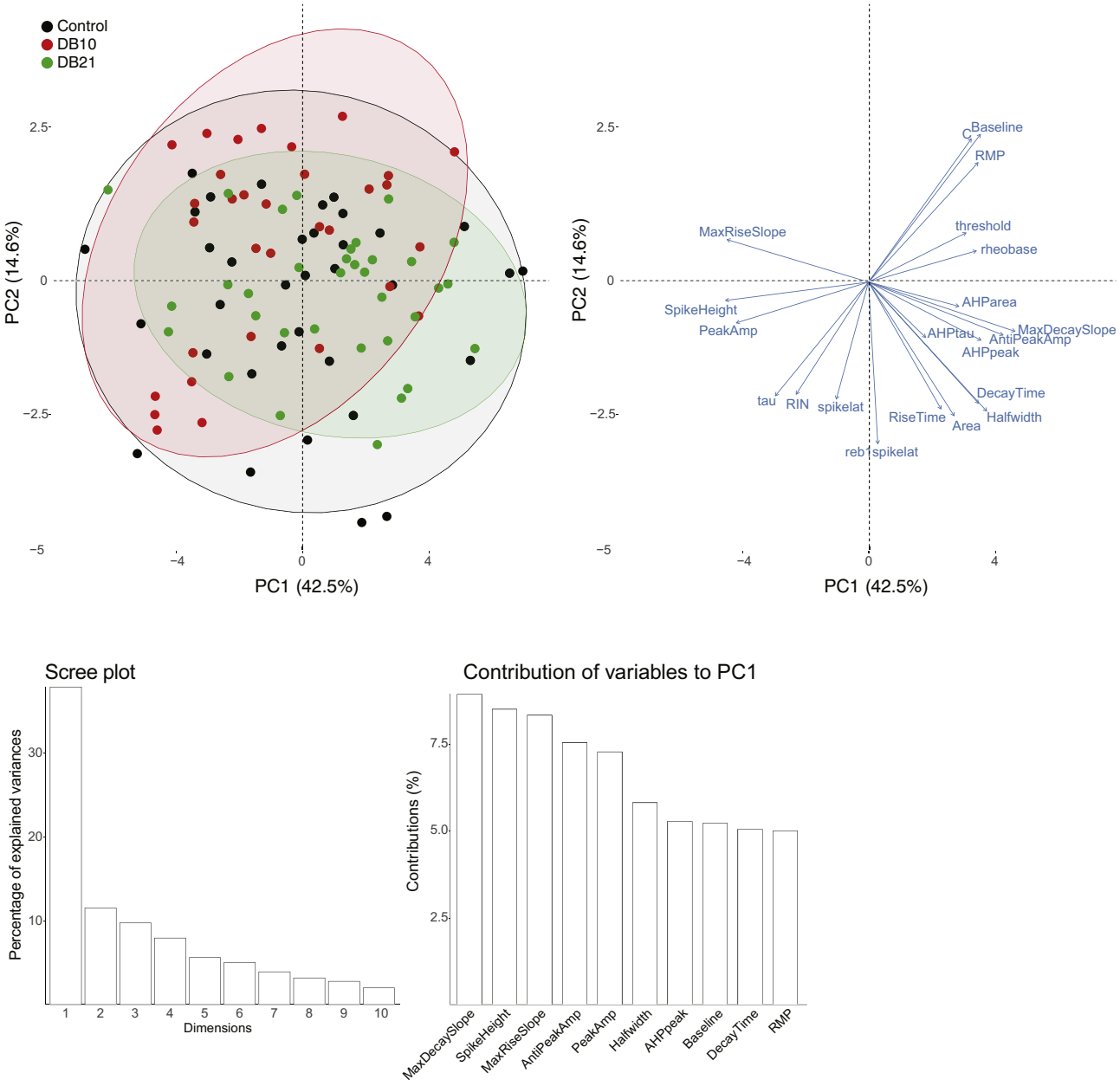


**Fig. 7.** Principal components analysis (PCA) of spike characteristics across WT, DB10, and DB21 mice. A. The first two principal components (PC1 and PC2) define the x-and y-axes respectively. PC1 accounted for 42.5% of the variance while PC2 accounted for 14.6%. By and large, all three groups show overlapping distribution of variance across PC1 and PC2. B. Scree plot demonstrating the amount of variance accounted for across the first 10 principal components. A substantial plurality of the variance is accounted for in the first principal component, while the remainder contribute far less to the variance in the data. C. Post-hoc analysis of the variables that contribute to the variance in PC1 reveals that relatively equal contributions are found from variables associated with spike shape and AHP amplitude.

measures of increased overall neuronal excitability. In contrast, week 21 Lepr$^{db/db}$ neurons changed in the opposite direction, exhibiting a decrease in spike probability and increased rheobase, both of which are indications of lower overall excitability. This trend of a change in firing properties at 10 weeks that is then rectified at 21 weeks is also seen in the characteristics of action potentials of MPG neurons. Specifically, spikes are narrower (as seen by a decreased half-width, increased ascending slope and enhanced decay slope in depolarization-induced spikes, and decreased decay time in DB10 animals), and AHPs are shorter are in the DB10 animals but return to control levels in the DB21 group. These data are consistent with the hypothesis that long-term diabetes results in changes in MPG neurons that are potentially compensated for via long-term plasticity mechanisms in the DB21 animals. Regardless of whether the changes in excitability and action potential properties are compensatory or represent disease progression in the context of the entire LUT, there are clear changes in the characteristics of MPG neurons over the course of 10–21 weeks in diabetic animals.

Although this study did not employ bladder tracing methods, it is interesting to note that the time course of changes in MPG neuron excitability mirror those of bladder output over the progression of diabetic cystopathy in rodents. For example, in type I diabetic mice there is a sharp decline in basal bladder pressure and mean threshold pressure from weeks 9–12 that then is rectified to control levels by 20 weeks (Daneshgari et al. 2006a). Similar time course changes in bladder output features as measured by cystometrogram have been documented in rats as well, whereby diabetic bladders transition from compensated to decompensated states between 9 and 12 weeks following onset of diabetes (Daneshgari et al. 2006b). Therefore, while a direct

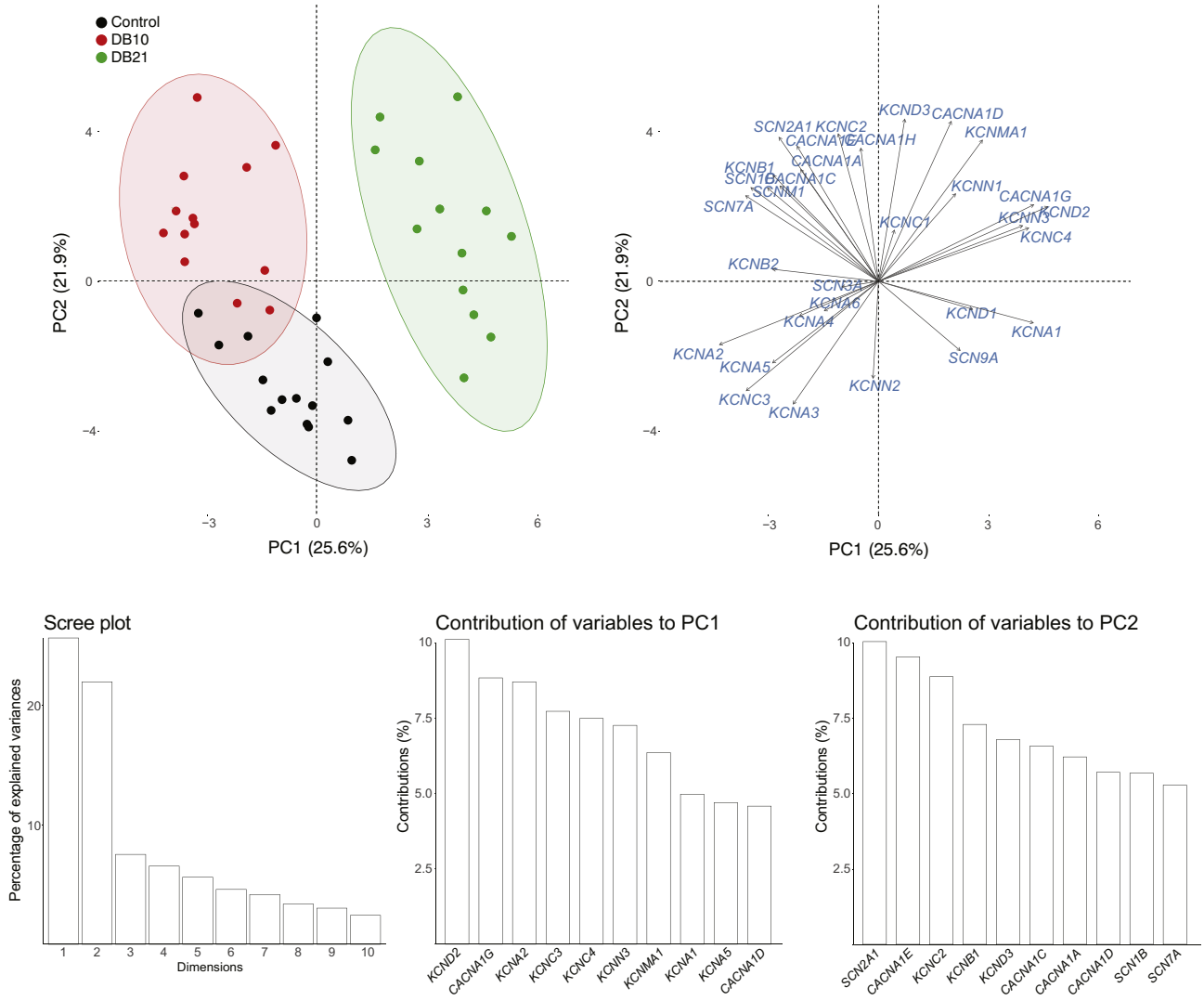


**Fig. 8.** PCA of ion channel mRNA levels across WT, DB10, and DB21 mice. A. The first two principal components (PC1 and PC2) define the x-and y-axes respectively. PC1 accounted for 25.6% of the variance while PC2 accounted for 21.9%. The distribution across PC1 and PC2 reveals three distinct ion channel expression profiles for WT, DB10, and DB21 animals. B. Scree plot demonstrating the amount of variance accounted for across the first 10 principal components. The majority of the variance is accounted for in the PC1 and PC2, while the remainder contribute far less to the variance in the data. C. Post-hoc analysis of the variables that contribute to the variance in PC1 and PC2 reveals distinct channel subunits that account for the distinct patterns of expression seen in all three experimental groups.

mechanistic link to bladder output cannot be made from our data, the results are consistent with the overall change in LUT output over the time course of diabetic cystopathy.

### *4.2. Potential mechanistic insights via interpretation of changes in mRNA levels*

It would be an over-interpretation to directly infer mechanisms underlying physiological changes in single neurons from data collected at the mRNA level from whole ganglia. However, the steady-state mRNA levels for ion channels provide a high-throughput opportunity to generate hypotheses regarding underlying mechanistic changes in ionic currents. Indeed, we see multiple changes in channel mRNAs that are consistent with the physiological changes we report. In this section, we will highlight some of the most salient changes we found at the level of neuronal properties, and cautiously hypothesize on potential underlying mechanism via changes at the mRNA level.

In 10-week Lepr$^{db/db}$ mice we observed that although rheobase did not change, several properties associated with excitability did change. The most salient of these properties was the increase of the probability of firing 2 or more spikes. As shown in Fig. 4A and also previously documented (Suzuki and Rogawski, 1989; Tompkins et al., 2013), MPG neurons can spike once or many times, a phenomena observed in many other autonomic neuron types (Cassell et al., 1986; Malin and Nerbonne 2001; Springer et al., 2015). One obvious possible mechanism for generating multiple spikes is the activation of a depolarizing current with somewhat slower kinetics that can maintain depolarization above threshold to allow for the generation of multiple spikes. Our data show changes in channel expression that are consistent with this hypothesis. In particular, there is a significant increase in mRNA levels for the calcium channels *CACNA1A, CACNA1E,* and *CACNA1H* in DB10 animals relative to both WT and DB21. Furthermore, *CACNA1E* levels overall are the most abundant calcium channel mRNA that we detected, with levels an order of magnitude higher than any other calcium channel subunit. *CACNA1E* encodes the R-type current $Ca_v2.3$, which is known to make up ~25% of total calcium current in rat MPG neurons (Won et al., 2006), and $Ca_v3.2$ – encoded by *CACNA1H* – is the predominant T-type channel in rat MPG (Lee et al., 2002). R-type currents are known to influence bursting output in CA1 pyramidal neurons (Metz et al., 2005), and T-type currents in many neurons trigger low-

threshold spikes, which in turn generate bursts of action potentials (Perez-Reyes, 2003). While the interplay of multiple calcium channel subunits and the remaining ionic conductances of the cell are quite complex in terms of generating different output patterns, increases in R-type and T-type currents would be a feasible way to influence the multiple spiking phenotype in DB10 animals.

We also observed increased ascending (in response to depolarizing current) and descending spike slopes, and decreased spike half-width in the DB10 animals relative to WT and DB21. We observed increased expression of mRNAs coding for $Na_v1.2$ (*SCN2A1*), as well as a trend for increased $Na_v\beta1$ (SCN1B) expression, in the DB10 animals. $Na_v1.2$ channels are largely localized to the axons and initial segments of unmyelinated neurons (Vacher et al., 2008), which is consistent with the post-ganglionic fibers of the MPG. $Na_v\beta1$ is known to interact with $Na_v1.2$ channels to increase surface expression of these subunits (Isom et al., 1995). Therefore, increases in expression of *SCN2A1* and *SCNB1* would be expected to increase AP upstroke, which was observed for depolarizing current injections but not rebound spikes. In addition, $K_v3.2$ and $K_v2.1$ are potassium channels with relatively high threshold activation and fast deactivation such that they have both been implicated as large contributors to the AP repolarization and as a consequence decrease AP width (Rudy and McBain, 2001; Liu and Bean, 2014). The upregulation of their constituent mRNA subunits (*KCNC2* and *KCNB1* respectively) is entirely consistent with the firing phenotypes observed.

As we observed increases in ascending spike slope to depolarizing current injections, but not rebound current injections in DB10 neurons, it is possible that high threshold potassium currents with fast deactivation time constants could play a role in permitting multiple spikes during depolarizing current injections by enhancing sodium channel de-inactivation. As Kv2 family members are known to encode delayed rectifiers, and Kv3 channels have fast activation and deactivation rates associated with sustained higher-frequency firing, then the fact that we see increased Kv3.2 (*KCNC2*) and Kv2.1 (*KCNB1*) expression is also consistent with these results. While this is well documented for Kv3.2 as it is a high threshold, fast deactivating (Weiser et al., 1994; Rudy and McBain, 2001) ion channel, it is less clear that this is the case for Kv2.1 as it is intermediate in these parameters. For example, in the superior cervical ganglion (SCG) neurons, Kv2.1 has somewhat high $V_{1/2}$ activation, slow activation, slow or no inactivation, but a relatively fast deactivation (Liu and Bean, 2014). If Kv2.1 is playing a role in keeping the functional pool of sodium channels available through de-inactivation, as it is thought to do in SCG neurons (Liu and Bean, 2014), then we expect its upregulation should prevent decay in spike height during a train of spikes. Therefore, to test this prediction, we examined the ratio of the 2nd to 1st spike height of multi-spiking neurons. A *t*-test showed that 2nd to 1st spike ratio of DB10 neurons ($0.79 \pm 0.03$, $n = 8$) were significantly less attenuated than WT neurons ($0.48 \pm 0.11$, $n = 2$) ($t(8) = -4.416$, $p = 0.002$). This suggests that together Kv3.2 and Kv2.1 could play a role in keeping sodium currents de-inactivated in the DB10 condition.

DB21 neurons were significantly less excitable than both DB10 and wild type neurons: rheobase was significantly increased, and $R_{IN}$ was significantly reduced compared to wildtype, and DB21 neurons did not produce a multi-spiking output when stimulated. DB21 neurons had significantly upregulated mRNAs encoding several low threshold slow deactivating potassium currents that would be expected to reduce excitability. The upregulation of *KCNA1* (Kv1.1) likely contributes to reduced excitability given a relatively low threshold of activation ($\sim -32$ mV) and intermediate deactivation time constant (Grissmer et al., 1994). The upregulation of *KCND2* (Kv4.2) is consistent with the observed decrease in excitability and may explain in part why the DB21 condition did not share the multispiking phenotype with DB10. This is because in cultured rat superior cervical ganglion neurons, Malin and Nerbonne (2000) showed that when Kv4.2 is overexpressed, the number of neurons displaying the multi-spiking neuron phenotype is decreased, and when the gene is downregulated by expression of a dominant negative transgene, there is a corresponding increase in the multi-spiking phenotype. Interestingly, the authors also report increased $R_{IN}$ in cells with reduced Kv4.2, and decreased $R_{IN}$ with overexpression of Kv4.2 (Malin and Nerbonne 2001) which is consistent with the significant decrease in $R_{in}$ in DB21 neurons.

### 4.3. Study limitations

In our study, we assumed there was no difference in WT mice from weeks 10 to 21 with the expectation that diabetic condition would only worsen with age. However, the findings shown here suggest that age is an important variable to consider during diabetes, and it would have been more informative to have an age control to rule out age-related changes. Despite this, we believe that while not ideal, there are several reasons to think that the contribution from age may be small. First, we saw no difference in metabolic parameters for WT mice, including weight, from weeks 10 to 21 (Fig. 2) suggesting that this study is in line with the ubiquitous assumption that the mature adult mouse is at the point at which 'development has ended but senescence has not yet begun" (Jackson et al., 2017). Further, certain types of adult urinary behavior are fully mature by 4–5 weeks in female C57BL/6J mice. Specifically, diurnal micturition variation, i.e. urinating more during the active period (night for mice), is shown to saturate to the adult pattern without further changes by 4–5 weeks (Negoro et al., 2013). Supporting this contention is that while there are copious articles on development and aging, there is a conspicuous absence of literature on changes occur during early adulthood. More importantly, when comparing the work of Tompkins et al. who studied 12–20 week and 26–28 week male C57BL6/J mice (Tompkins et al., 2010, 2013); the measured properties RMP, AHP, and AHP duration did not appear to be different, and only $R_{IN}$ is believed to increase during this time period. This suggests that with exception of $R_{IN}$, the impact of age on these properties is minimal. In the case of our finding of reduced $R_{IN}$ in WT21 females, an age control would be expected to increase, and therefore we have *underestimated* this effect if there are no sex differences.

A potential limitation of this study is that it was done at room temperature rather than physiological temperature. While it is difficult to make direct mechanistic interpretations at non-physiological temperature, these experiments clearly implicate changes in excitability of MPG neurons as part of the progression of type II diabetes.

We observed fewer multispiking neurons than reported in other studies. As the proportion of multispiking cells have shown to be androgen dependent in rat (Kanjhan et al., 2003), our study is not directly comparable to (Tompkins et al., 2013) who studied male mice. However, previous estimates of multispiking neurons in female C57BL/6J MPG neurons are about 28.6% (14/49 neurons) (Jobling and Lim, 2008) while we only observed about 5.4% in WT neurons (2/37 neurons). We are uncertain if this difference is due to variability, temperature or "impalement damage." As this study was conducted at room temperature, while previous studies were conducted at 35 °C (Jobling and Lim, 2008) differences in temperature sensitivity of conductances could alter firing phenotype. This is because activation and inactivation parameters can have different Q10s (Tang et al., 2010), which as a consequence can alter conductances and thus excitability (Cuevas et al., 1997; Tang et al., 2010; Wang et al., 2011). Another possibility is that impalement damage has led to a lower proportion of multispiking neurons than expected. Although some studies argue that impalement damage from sharp electrodes may affect measured passive properties while leaving excitability unchanged (Li et al., 2004), there are examples where introduction of leak reduces excitability (Cymbalyuk and Shilnikov, 2005; Springer et al., 2015). For example, Springer et al. (2015) showed that injection of artificial leak into multispiking neurons with dynamic clamp can transform them into phasic cells. Interestingly, however, the converse is not true, as this same study showed that not all phasic cells can be transformed into tonic cells by injection of negative

leak. Therefore, it is possible – but difficult to determine – that impalement damage could explain the lower rate of multispiking neurons observed in the present study versus that of Jobling and Lim (2008). As the goal of this study was to compare across diabetic condition, impalement damage could explain our lower observation of multispiking cells in WT, but not why DB10 had more multispiking cells than WT as recording conditions and electrodes were consistent throughout. Therefore, comparisons across groups strongly suggest an effect of diabetes on the spiking properties and excitability of these neurons.

Finally, mRNA does not represent mature and functional protein, and so at best, the link between our gene expression data and physiology is inferential. This is further limited by the fact that we performed electrophysiology on individual neurons, but mRNA are gathered from the entire (heterogeneous) population of MPG cells. Therefore, while the mRNA data allow us to generate hypotheses with respect to mechanism, these must be tested at the single cell physiological level through more direct means.

## 5. Conclusions

We expected excitability of $Lepr^{db/db}$ neurons to change with increasing intensity from weeks 10 to 21 as diabetes progressed; as diabetic neuropathy is a function of both hyperglycemia and duration in humans (Maser et al., 1989; Davies et al., 2006), rats (Mattingly and Fischer, 1983; Sasaki et al., 2002) and mice (Giachetti, 1978; Hinder et al., 2017; Liu et al., 2017). Contrary to this hypothesis, many properties associated with excitability changed in 10-week animals, but were then resolved closer to wild-type levels in the 21-week animals. These properties include both characteristics of intrinsic excitability (e.g. probability to fire, threshold, and rebound latency) as well as many of the characteristics of the individual action potentials of these neurons as well. Yet, our expression profiling of the MPGs does not simply reveal a resolution at 21-weeks of changes in expression that occur in the 10-week animals. Rather, our PCA reveals that the overall expression patterns in MPGs of wild type, 10-week, and 21-week animals are entirely distinct. Taken together, we suggest that these results provide further evidence for a direct effect of the diabetic phenotype on the properties of peripheral autonomic neurons (Tompkins et al., 2013), including differences between younger diabetic mice that are less adapted to hyperglycemia and older diabetic mice that have been exposed to hyperglycemia for longer times.

## Acknowledgments

This work was funded by a grant from the Missouri Spinal Cord Injuries Research Program (D.J.S.), the Craig H. Neilsen Foundation (D.J.S.), American Diabetes Association Grant 1-14-BS-181 (L.C.S.) and American Heart Association Postdoctoral Fellowship 13POST16910108 (K.A.P.). The authors declare no competing financial interests.

## References

Breyer, M.D., Bottinger, E., Brosius 3rd, F.C., Coffman, T.M., Harris, R.C., Heilig, C.W., Sharma, K., Amdcc, 2005. Mouse models of diabetic nephropathy. J Am Soc Nephrol 16, 27–45.

Boddum, K., Hougaard, C., Xiao-Ying Lin, J., von Schoubye, N.L., Jensen, H.S., Grunnet, M., Jespersen, T., 2017. Kv3.1/Kv3.2 channel positive modulators enable faster activating kinetics and increase firing frequency in fast-spiking GABAergic interneurons. Neuropharmacology 118, 102–112.

Cassell, J.F., Clark, A.L., McLachlan, E.M., 1986. Characteristics of phasic and tonic sympathetic ganglion cells of the guinea-pig. J. Physiol. 372, 457–483.

Chen, H., Charlat, O., Tartaglia, L.A., Woolf, E.A., Weng, X., Ellis, S.J., Lakey, N.D., Culpepper, J., Moore, K.J., Breitbart, R.E., Duyk, G.M., Tepper, R.I., Morgenstern, J.P., 1996. Evidence that the diabetes gene encodes the leptin receptor: identification of a mutation in the leptin receptor gene in db/db mice. Cell 84, 491–495.

Cuevas, J., Harper, A.A., Trequattrini, C., Adams, D.J., 1997. Passive and active membrane properties of isolated rat intracardiac neurons: regulation by H- and M-currents. J. Neurophysiol. 78, 1890–1902.

Cymbalyuk, G., Shilnikov, A., 2005. Coexistence of tonic spiking oscillations in a leech neuron model. J. Comput. Neurosci. 18, 255–263.

Dale, N., 1995. Experimentally derived model for the locomotor pattern generator in the Xenopus embryo. J. Physiol. 489 (Pt 2), 489–510.

Daneshgari, F., Huang, X., Liu, G., Bena, J., Saffore, L., 2006. Powell CT. Temporal differences in bladder dysfunction caused by diabetes, diuresis, and treated diabetes in mice. Am J Physiol Regul Integr Comp Physiol 290 (6), R1728–1735 PubMed PMID: 16439670.

Davies, M., Brophy, S., Williams, R., Taylor, A., 2006. The prevalence, severity, and impact of painful diabetic peripheral neuropathy in type 2 diabetes. Diabetes Care 29, 1518–1522.

Daneshgari, F., Liu, G., Imrey, PB., 2006b. Time dependent changes in diabetic cystopathy in rats include compensated and decompensated bladder function. J Urol 176 (1), 380–386 PubMed PMID: 16753447.

DCCT Research Group t, 1996. The absence of a glycemic threshold for the development of long-term complications: the perspective of the Diabetes Control and Complications Trial. Diabetes 45, 1289–1298.

Faerman, I., Maler, M., Jadzinsky, M., Alvarez, E., Fox, D., Zilbervarg, J., Cibeira, J.B., Colinas, R., 1971. Asymptomatic neurogenic bladder in juvenile diabetics. Diabetologia 7, 168–172.

Felix, B., Catalin, D., Miolan, J.P., Niel, J.P., 1998. Integrative properties of the major pelvic ganglion in the rat. J. Auton. Nerv. Syst. 69, 6–11.

Frimodt-Moller, C., 1980. Diabetic cystopathy: epidemiology and related disorders. Ann. Intern. Med. 92, 318–321.

Garcia, V.B., Garcia, M.L., Schulz, D.J., 2014. Quantitative expression profiling in mouse spinal cord reveals changing relationships among channel and receptor mRNA levels across postnatal maturation. Neuroscience 277, 321–333.

Garcia, V.B., Abbinanti, M.D., Harris-Warrick, R.M., Schulz, D.J., 2018. Effects of chronic spinal cord injury on relationships among ion channel and receptor mRNAs in mouse lumbar spinal cord. Neuroscience 393, 42–60.

Giachetti, A., 1978. The functional state of sympathetic nerves in spontaneously diabetic mice. Diabetes 27, 969–974.

Golowasch, J., Thomas, G., Taylor, A.L., Patel, A., Pineda, A., Khalil, C., Nadim, F., 2009. Membrane capacitance measurements revisited: dependence of capacitance value on measurement method in nonisopotential neurons. J. Neurophysiol. 102, 2161–2175.

Grissmer, S., Nguyen, A.N., Aiyar, J., Hanson, D.C., Mather, R.J., Gutman, G.A., Karmilowicz, M.J., Auperin, D.D., Chandy, K.G., 1994. Pharmacological characterization of five cloned voltage-gated K+ channels, types Kv1.1, 1.2, 1.3, 1.5, and 3.1, stably expressed in mammalian cell lines. Mol. Pharmacol. 45, 1227–1234.

Gunnarsson, R., 1975. Function of the pancreatic B-cell during the development of hyperglycaemia in mice homozygous for the mutations "diabetes" (db) and "misty" (m). Diabetologia 11, 431–438.

Hanani, M., 2010. Satellite glial cells in sympathetic and parasympathetic ganglia: in search of function. Brain Res. Rev. 64, 304–327.

Hinder, L.M., O'Brien, P.D., Hayes, J.M., Backus, C., Solway, A.P., Sims-Robinson, C., Feldman, E.L., 2017. Dietary reversal of neuropathy in a murine model of prediabetes and metabolic syndrome. Dis. Model. Mech. 10, 717–725.

Hummel, K.P., Coleman, D.L., Lane, P.W., 1972. The influence of genetic background on expression of mutations at the diabetes locus in the mouse. I. C57BL-KsJ and C57BL-6J strains. Biochem. Genet. 7, 1–13.

Isom, L.L., Scheuer, T., Brownstein, A.B., Ragsdale, D.S., Murphy, B.J., Catterall, W.A., 1995. Functional co-expression of the beta 1 and type IIA alpha subunits of sodium channels in a mammalian cell line. J. Biol. Chem. 270, 3306–3312.

Jackson, S.J., Andrews, N., Ball, D., Bellantuono, I., Gray, J., Hachoumi, L., Holmes, A., Latcham, J., Petrie, A., Potter, P., Rice, A., Ritchie, A., Stewart, M., Strepka, C., Yeoman, M., Chapman, K., 2017. Does age matter? The impact of rodent age on study outcomes. Lab. Anim. 51, 160–169.

Jobling, P., Lim, R., 2008. Anatomical and physiological properties of pelvic ganglion neurons in female mice. Autonomic neuroscience: basic & clinical 140, 30–39.

Kanjhan, R., Osborne, P.B., Ouyang, M., Keast, J.R., 2003. Postnatal maturational changes in rat pelvic autonomic ganglion cells: a mixture of steroid-dependent and -independent effects. J. Neurophysiol. 89, 315–323.

Kaplan, S.A., Te, A.E., Blaivas, J.G., 1995. Urodynamic findings in patients with diabetic cystopathy. J. Urol. 153, 342–344.

Keast, J.R., 1995. Visualization and immunohistochemical characterization of sympathetic and parasympathetic neurons in the male rat major pelvic ganglion. Neuroscience 66, 655–662.

Keast, J.R., 2006. Plasticity of pelvic autonomic ganglia and urogenital innervation. Int. Rev. Cytol. 248, 141–208.

Kebapci, N., Yenilmez, A., Efe, B., Entok, E., Demirustu, C., 2007. Bladder dysfunction in type 2 diabetic patients. Neurourol. Urodyn. 26, 814–819.

Lee, J.H., Kim, E.G., Park, B.G., Kim, K.H., Cha, S.K., Kong, I.D., Lee, J.W., Jeong, S.W., 2002. Identification of T-type alpha1H Ca2+ channels (Ca(v)3.2) in major pelvic ganglion neurons. J. Neurophysiol. 87, 2844–2850.

Li, W.C., Soffe, S.R., Roberts, A., 2004. A direct comparison of whole cell patch and sharp electrodes by simultaneous recording from single spinal neurons in frog tadpoles. J. Neurophysiol. 92, 380–386.

Liu, P.W., Bean, B.P., 2014. Kv2 channel regulation of action potential repolarization and firing patterns in superior cervical ganglion neurons and hippocampal CA1 pyramidal neurons. J. Neurosci. 34, 4991–5002.

Liu, Y., Sebastian, B., Liu, B., Zhang, Y., Fissel, J.A., Pan, B., Polydefkis, M., Farah, M.H., 2017. Sensory and autonomic function and structure in footpads of a diabetic mouse model. Sci. Rep. 7, 41401.

Malin, S.A., Nerbonne, J.M., 2000. Elimination of the fast transient in superior cervical ganglion neurons with expression of KV4.2W362F: molecular dissection of IA. J. Neurosci. Off. J. Soc. Neurosci. 20, 5191–5199.

Maser, R.E., Steenkiste, A.R., Dorman, J.S., Nielsen, V.K., Bass, E.B., Manjoo, Q., Drash, A.L., Becker, D.J., Kuller, L.H., Greene, D.A., et al., 1989. Epidemiological correlates

of diabetic neuropathy. Report from Pittsburgh Epidemiology of Diabetes Complications Study. Diabetes 38, 1456–1461.
Malin, S.A., Nerbonne, JM., 2001. Molecular heterogeneity of the voltage-gated fast transient outward K+ current, I(Af), in mammalian neurons. J Neurosci 21 (20), 8004–8014 PubMed PMID: 11588173.
Mattingly, G.E., Fischer, V.W., 1983. Peripheral neuropathy following prolonged exposure to streptozotocin-induced diabetes in rats: a teased nerve fiber study. Acta Neuropathol. 59, 133–138.
Medici, F., Hawa, M., Ianari, A., Pyke, D.A., Leslie, R.D., 1999. Concordance rate for type II diabetes mellitus in monozygotic twins: actuarial analysis. Diabetologia 42, 146–150.
Metz, A.E., Jarsky, T., Martina, M., Spruston, N., 2005. R-type calcium channels contribute to afterdepolarization and bursting in hippocampal CA1 pyramidal neurons. J. Neurosci. Off. J. Soc. Neurosci. 25, 5763–5773.
Nadelhaft, I., Vera, P.L., 1992. Reduced urinary bladder afferent conduction velocities in streptozocin diabetic rats. Neurosci. Lett. 135, 276–278.
Naundorf, B., Wolf, F., Volgushev, M., 2006. Unique features of action potential initiation in cortical neurons. Nature 440, 1060–1063.
Negoro, H., Kanematsu, A., Matsuo, M., Okamura, H., Tabata, Y., Ogawa, O., 2013. Development of diurnal micturition pattern in mice after weaning. J. Urol. 189, 740–746.
Perez-Reyes, E., 2003. Molecular physiology of low-voltage-activated t-type calcium channels. Physiol. Rev. 83, 117–161.
Platkiewicz, J., Brette, R., 2010. A threshold equation for action potential initiation. PLoS Comput. Biol. 6, e1000850.
Platkiewicz, J., Brette, R., 2011. Impact of fast sodium channel inactivation on spike threshold dynamics and synaptic integration. PLoS Comput. Biol. 7, e1001129.
Rudy, B., McBain, C.J., 2001. Kv3 channels: voltage-gated K+ channels designed for high-frequency repetitive firing. Trends Neurosci. 24, 517–526.
Sasaki, K., Chancellor, M.B., Phelan, M.W., Yokoyama, T., Fraser, M.O., Seki, S., Kubo, K., Kumon, H., Groat, W.C., Yoshimura, N., 2002. Diabetic cystopathy correlates with a long-term decrease in nerve growth factor levels in the bladder and lumbosacral dorsal root Ganglia. J. Urol. 168, 1259–1264.
Sasaki, K., Chancellor, M.B., Goins, W.F., Phelan, M.W., Glorioso, J.C., de Groat, W.C., Yoshimura, N., 2004. Gene therapy using replication-defective herpes simplex virus vectors expressing nerve growth factor in a rat model of diabetic cystopathy. Diabetes 53, 2723–2730.
Spandidos, A., Wang, X., Wang, H., Seed, B., 2010. PrimerBank: a resource of human and mouse PCR primer pairs for gene expression detection and quantification. Nucleic Acids Res. 38, D792–D799.
Springer, M.G., Kullmann, P.H., Horn, J.P., 2015. Virtual leak channels modulate firing dynamics and synaptic integration in rat sympathetic neurons: implications for ganglionic transmission in vivo. J. Physiol. 593, 803–823.
Sullivan, K.A., Hayes, J.M., Wiggin, T.D., Backus, C., Su Oh, S., Lentz, S.I., Brosius 3rd, F., Feldman, E.L., 2007. Mouse models of diabetic neuropathy. Neurobiol. Dis. 28, 276–285.
Suzuki, S., Rogawski, M.A., 1989. T-type calcium channels mediate the transition between tonic and phasic firing in thalamic neurons. Proc. Natl. Acad. Sci. U. S. A. 86, 7228–7232.
Tan, H., Mawe, G.M., Vizzard, M.A., 2007. Electrical properties of neurons in the intact rat major pelvic ganglion. Autonomic neuroscience: basic & clinical 134, 26–37.
Tang, L.S., Goeritz, M.L., Caplan, J.S., Taylor, A.L., Fisek, M., Marder, E., 2010. Precise temperature compensation of phase in a rhythmic motor pattern. PLoS Biol. 8.
Tompkins, J.D., Girard, B.M., Vizzard, M.A., Parsons, R.L., 2010. VIP and PACAP effects on mouse major pelvic ganglia neurons. Journal of molecular neuroscience: MN 42, 390–396.
Tompkins, J.D., Vizzard, M.A., Parsons, R.L., 2013. Synaptic transmission at parasympathetic neurons of the major pelvic ganglion from normal and diabetic male mice. J. Neurophysiol. 109, 988–995.
UKPDS, 1998. Intensive blood-glucose control with sulphonylureas or insulin compared with conventional treatment and risk of complications in patients with type 2 diabetes (UKPDS 33). UK Prospective Diabetes Study (UKPDS) Group. Lancet 352, 837–853.
United States. Department of Health and Human Services., Center for Disease Control., and National Center for Health Statistics (U.S.), 2016. Health, United States, 2016: With Chartbook on Long-Term Trends in Health. National Center for Health Statistics, Hyattsville, MD (p. xv, 476 pages.).
Vacher, H., Mohapatra, D.P., Trimmer, J.S., 2008. Localization and targeting of voltage-dependent ion channels in mammalian central neurons. Physiol. Rev. 88, 1407–1447.
Vandesompele, J., De Preter, K., Pattyn, F., Poppe, B., Van Roy, N., De Paepe, A., Speleman, F., 2002. Accurate normalization of real-time quantitative RT-PCR data by geometric averaging of multiple internal control genes. Genome Biol. 3 RESEARCH 0034.
Vinik, A.I., Maser, R.E., Mitchell, B.D., Freeman, R., 2003. Diabetic autonomic neuropathy. Diabetes Care 26, 1553–1579.
Vinik, A.I., Maser, R.E., Ziegler, D., 2011. Autonomic imbalance: prophet of doom or scope for hope? Diabetic medicine: a journal of the British Diabetic Association 28, 643–651.
Wang, Y.Y., Qin, J., Han, Y., Cai, J., Xing, G.G., 2011. Hyperthermia induces epileptiform discharges in cultured rat cortical neurons. Brain Res. 1417, 87–102.
Wang, B., Chandrasekera, P.C., Pippin, J.J., 2014. Leptin- and leptin receptor-deficient rodent models: relevance for human type 2 diabetes. Curr. Diabetes Rev. 10, 131–145.
Weiser, M., De Miera, E.V.S., Kentros, C., Moreno, H., Franzen, L., Hillman, D., Baker, H., Rudy, B., 1994. Differential expression of Shaw-related K+ channels in the rat central nervous system. J. Neurosci. Off. J. Soc. Neurosci. 14, 949–972.
White, W.E., Hooper, S.L., 2013. Contamination of current-clamp measurement of neuron capacitance by voltage-dependent phenomena. J. Neurophysiol. 110, 257–268.
Won, Y.J., Whang, K., Kong, I.D., Park, K.S., Lee, J.W., Jeong, S.W., 2006. Expression profiles of high voltage-activated calcium channels in sympathetic and parasympathetic pelvic ganglion neurons innervating the urogenital system. J. Pharmacol. Exp. Ther. 317, 1064–1071.
Yuan, Z., Tang, Z., He, C., Tang, W., 2015. Diabetic cystopathy: a review. Journal of diabetes 7, 442–447.